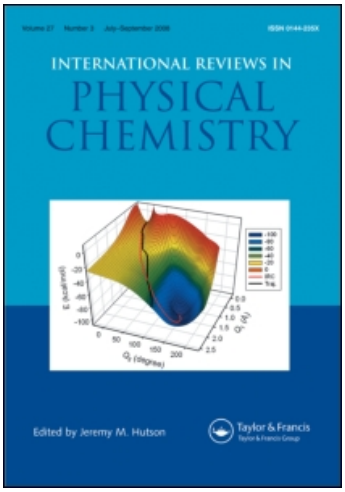

International Reviews in Physical Chemistry
Publication details, including instructions for authors and subscription information:
http://www.informaworld.com/smpp/title~content=t713724383

Dynamics of reactive collisions by optical methods

A. González Ureña[a]; R. Vetter[b]
[a] Instituto Pluridisciplinar, Universidad Complutense, Madrid, Spain [b] Laboratoire Aimé Cotton, Orsay, Cedex, France

To cite this Article Ureña, A. González and Vetter, R.(1996) 'Dynamics of reactive collisions by optical methods', International Reviews in Physical Chemistry, 15: 2, 375 — 427
To link to this Article: DOI: 10.1080/01442359609353189
URL: http://dx.doi.org/10.1080/01442359609353189

INTERNATIONAL REVIEWS IN PHYSICAL CHEMISTRY, 1996, VOL. 15, NO. 2, 375–427

Dynamics of reactive collisions by optical methods

by A. GONZÁLEZ UREÑA†
Instituto Pluridisciplinar, Universidad Complutense, Paseo Juan XXIII, 1, 28040 Madrid, Spain

and R. VETTER
Laboratoire Aimé Cotton, CNRS II, Bat. 505, Campus d'Orsay, 91405 Orsay Cedex, France

This paper reviews recent developments in the study of reactive collisions using optical methods. Although the basic approach is from the experimental viewpoint, attention is paid to the conceptual and theoretical aspects of the physics underlying modern reaction dynamics. After a brief resumé of basic concepts and definitions on both scalar and vectorial quantities characterizing the chemical reaction, a significant body of this paper describes the recent achievements using laser techniques, mainly via laser-induced fluorescence, and chemiluminescence. Both high-resolution crossed-beam and high-resolution bulb studies are presented in a complementary fashion, as they provide a detailed picture of reaction dynamics through the measurement of quantum state specific differential cross-sections. Specific examples include the use of Doppler resolved laser-induced fluorescence, multiphoton ionization or CARS studies. Some examples are also included based on the use of product imaging techniques, the novel approach of obtaining quantum state resolved differential cross-sections for chemical reactions. In addition, new data on the collision energy dependence of the collision cross-section, i.e. the excitation function, obtained by highly sensitive collision energy cross-beam techniques is also presented and reviewed. Another part of the paper is dedicated to recent advances in the study of reaction dynamics using electronically excited species. Emphasis is placed not only on the opening of new channels for chemical reactions but also on the possible outcome of the reaction products associated with the different symmetries of the excited potential energy surfaces. Finally, a section is dedicated to recent developments in studies carried out in the area of van der Waals and cluster reactions. The possibility of clocking the chemical act as well as very efficient trapping of reaction intermediates is illustrated with some examples. Throughout the whole paper care is taken to discuss the most significant features of the molecular reaction dynamic observables with reference to simple reaction models and/or theoretical treatments currently used in the field.

1. Introduction

Reaction dynamics is a major subdiscipline of a wide field of research—molecular dynamics—which is concerned with both intramolecular motions and intermolecular collisions. The fundamental aim of reaction dynamics is to understand the intimate mechanisms of chemical reactivity, at the most elementary level of individual, isolated, gas-phase collisions (Fluendy and Lawley 1973, Polanyi and Schreiber 1974, Child 1974, Toennies 1974, Smith 1980, Berry *et al.* 1980, Bernstein 1982, 1984, Levine and Bernstein 1987, Scoles 1988, Gonzalez Urena 1991). Experimentally, it is necessary to control the various parameters which determine the fate of the collision and to probe

† FBBV Visiting Professor in the Chemistry Department of the University of Cambridge during 1995.

0144–235X/96 $12·00

the reaction products in their nascent states, under the so-called 'single-collision' conditions which are typically provided by cross-beam experiments. Theoretically, the first requirement is to calculate the potential energy of the reactive system by the use of quantum chemistry techniques and to carry out its collision dynamics using classical and/or quantum methods. Until now, these calculations have been reliable only for simple systems—generally in their ground state—thus the detailed comparison between theory and experiment is still rather limited. However, although restricted to simple systems involving a small number of atoms and electrons, experiments and calculations performed since the beginning of the 1960s have led to the understanding of the main features of reaction dynamics—among which the angular scattering of products is perhaps the most striking—and to the concept of realistic collision models. The challenge now is to extend this knowledge to chemical systems of interest for astrophysics, the environment, combustion, catalysis, and many other fields, which are outside the scope of this paper.

Optical methods have played an important part in the development of these experiments, as they are well-suited for state-selected and state-resolved studies of elementary chemical reactions (Bernstein 1982). For instance, it has been shown since the very beginning that exoergic reactions involving alkali atoms and halogen molecules give rise to an intense emission of chemiluminescence whose spectral analysis yields detailed information about reaction mechanisms and cross-sections. With the advent of laser sources, experimentalists have had access to a sophisticated tool with which to widen the field of reaction dynamics. In the area of high resolution, for example, the use of cw tunable lasers in crossed-beam experiments has allowed for the selective electronic excitation of atomic/molecular reagents and for the full characterization of reaction products (Odiorne *et al.* 1971, Arnoldi and Wolfrum 1976, Stolte *et al.* 1977, Zandee and Bernstein 1978, Vernon *et al.* 1986, Weiss *et al.* 1986, Billy *et al.* 1986, Rahmat *et al.* 1986, Loesch 1986, Mestdagh *et al.* 1987, Dagdigian and Campbell 1987, Whitehead 1988, Husain and Roberts 1989). New effects connected with light polarization have been observed, which are able to yield a deep insight into the stereodynamics of the reaction (Rettner and Zare 1981, 1982, Menzinger 1988, Davis *et al.* 1990). In another area—time-resolved spectroscopy—the use of very short laser pulses has led to the real-time dissociation dynamics of simple molecular systems (Zewail 1988, 1989). Generally speaking, optical techniques are powerful and versatile tools to study reaction dynamics under well-specified conditions but their application is obviously limited to those systems whose spectroscopy is well-known.

The present paper aims to provide an overview of the recent developments carried out in the dynamics of reactive collisions through the use of these optical methods. The approach used throughout this paper is close to the experimentalist's viewpoint, although results are always discussed in the light of current theories and relevant dynamical models. Chemiluminescence and laser-induced fluorescence techniques applied to beam-gas and crossed-beam experiments are treated preferentially, partly because they are more familiar to the authors' own research activity. Due to obvious limitations in the scope of a review paper, the rapid developments in gas–surface reaction dynamics are not treated here; the reader is directed to the recent Faraday Discussion No. 96 for an exciting overview of this field.

Total and differential cross-sections are important data for characterizing the features of reaction dynamics, and they constitute accurate tests for the detailed comparison between theory and experiment. However, these quantities can be of

different natures: for instance, a number is measured in the case of total absolute cross-sections whereas a shape is required in the case of angular differential cross-sections. Besides, the experimental arrangements currently used in reaction dynamics offer contrasting characteristics which determine the very nature of the measurements; for instance, total absolute cross-section measurements are better achieved in gas cells or with beam-gas arrangements whereas angular differential cross-sections are better defined and measured with cross-beam experiments. Therefore it appears necessary to clearly identify the basic concepts and definitions used in reaction dynamics: this is the subject of §2 of the present paper. Various optical techniques are then presented and discussed in terms of their ability to characterize the state of reaction products, in §3 by the use of lasers and in §4 through the analysis of chemiluminescence. In §5 it is shown how it is possible to obtain detailed information about the dynamics and stereodynamics of elementary chemical processes from the selective excitation of atomic/molecular reagents. Concluding remarks and new developments are presented in §6.

2. Basic definitions and concepts

Let us assume an 'ideal' single-collision experimental set-up where all the reagent parameters which determine the fate of the reactive collision are under control and where the product states are fully characterized in their nascent states. Relevant reagent parameters involve the kinetic energy, the internal energy as determined by usual atom/molecule quantum numbers, the impact parameter, and the mutual orientation in the centre-of-mass (c.m.). The full characterization of product states deals with the efficiency of the collisional process, the energy partitioning (i.e. the various kinetic, electronic, vibrational and rotational distributions), the angular scattering in c.m. and the vectorial properties of the system through correlations between reagent and product angular momenta. An ideal 'state-to-state' experiment would involve all these parameters and observables, hence detailed singly-, doubly-, triply-, etc. differential cross-sections whose measurement strongly depends upon the characteristics of the set-up. Unfortunately, such an experiment does not yet exist, although recent developments allow for an increasingly detailed approach to the reactive process: for example, the impact parameter is still out of reach even in the most sophisticated cross-beam experiment, but it is possible to indirectly study its influence in well-chosen kinematically-constrained reactions through the determination of the 'opacity function' (Noda *et al.* 1986).

2.1. *Scalar quantities: cross-sections*

The *total absolute cross-section* σ_R measures the efficiency of the overall reactive process. For an $A + BC \rightarrow AB + C$ bimolecular reaction studied under single-collision conditions, it is usually defined as follows for a unique reaction path between well-defined reagent states and well-defined product states

$$\sigma_R = \left(\frac{dN_{AB}}{dt}\right)(n_A n_{BC} V_r \Delta V)^{-1} \tag{1}$$

where dN_{AB}/dt is the total number of AB molecules created per second at the collision volume (or the total flux F_{AB} of product particles), n_A and n_{BC} are the number densities of reagent particles, V_r is the relative velocity of reagents and ΔV is the cross volume. From this definition, the total cross-section depends only upon scalar quantities; it corresponds to the interparticle size inside which any bimolecular collision gives rise

to atomic rearrangement. Typical reaction cross-sections range between 100 Å^2 and 0·01 Å^2, examples being provided by exoergic reactions between alkalis and halogens and by exchange reactions between hydrogen and deuterium respectively. Cross-sections are generally a function of the reagent kinetic energy E_T through the *excitation function*, $\sigma_R(E_T)$; they are related to reaction rate constants $k(T)$ by convoluting $\sigma_R(E_T)$ with a Maxwell–Boltzmann velocity distribution:

$$k(T) = (\pi\mu)^{-1/2}\left(\frac{2}{k_B T}\right)^{3/2}\int \sigma_R(E_T)\exp\left(\frac{-E_T}{k_B T}\right)dE_T \tag{2}$$

where k_B is the Boltzmann constant and μ is the reduced mass of the reagents. Equation (2) is the basic link between microscopic dynamics and macroscopic kinetics; it holds true assuming that the excitation function depends on the collision energy only. There is no complete equivalence between $\sigma_R(E_T)$ and $k(T)$, the determination of $\sigma_R(E_T)$ from $k(T)$ being difficult and less accurate than the reverse process.

As said before, the success of cross-beam scattering experiments has been to show that the reaction cross-section does involve vectorial quantities. Considering that the total F_{AB} of reaction products is independent of the coordinate system, one can introduce the flux of AB products scattered per unit time per unit solid angle in the centre-of-mass direction (θ, ϕ) as

$$F_{AB}(\theta, \phi) = n_A n_{BC} V_r \Delta V \sigma_R P(\theta, \phi) \tag{3}$$

The product $\sigma_R P(\theta, \phi)$ is called the *differential (solid angle) cross-section* with dimensions of area per unit solid angle: $\sigma_R P(\theta, \phi) = d^2\sigma/d^2\omega$, where $d^2\omega = \sin\theta\, d\theta\, d\phi$. $P(\theta)$ is the (normalized) probability density that products have to scatter at the angle θ with respect to the initial relative velocity.

For a spherically symmetrical potential there is no azimuthal dependence of the scattered intensity per unit solid angle and one can calculate the *differential (polar) cross-section*, which represents the fractional contribution to σ_R from any polar angle θ, by integrating over the azimuthal angle

$$\frac{d\sigma}{d\theta} = \int\left(\frac{d^2\sigma}{d^2\omega}\right)\sin\theta\, d\phi = 2\pi(d^2\sigma/d^2\omega)\sin\theta. \tag{4}$$

Hence, the total cross-section can be obtained as

$$\sigma_R = \int\left(\frac{d\sigma}{d\theta}\right)d\theta = \int 2\pi\left(\frac{d^2\sigma}{d^2\omega}\right)\sin\theta\, d\theta = \int 2\pi\sigma_R P(\theta)\sin\theta\, d\theta. \tag{5}$$

Of course, the differential cross-section $\sigma_R(\theta) = \sigma_R P(\theta)$ is a function of the collision energy and should be written as $\sigma_R(E_T, \theta)$, the *differential (solid angle) excitation function*.

Very often the experimental measurement of the differential cross-section is restricted to that of $P(\theta)$ whose shape is characteristic of the reaction mechanism. For instance, it was admitted long ago that the well-known harpooning mechanism which is relevant for direct reactions between alkalis and halogens gives rise to 'forward' scattering, i.e. scattering along the velocity of the incoming atom in c.m. This is because the jump of the alkali outer electron onto the neutral molecular partner occurs at large internuclear distances. Conversely, the 'rebound' mechanism which holds for the reaction between potassium and methyl iodide gives rise to 'backward' scattering.

Symmetrical scattering in c.m. is often characteristic of a non-direct reaction, with formation of an intermediate complex whose lifetime is comparable with its rotational period.

Another type of differential cross-section results when the product translational energy distribution is considered, that is $P(E'_T)$. Now $\sigma_R(E'_T) = \sigma_R P(E'_T)$ is the *differential cross-section for scattering into a given final translational energy*. By analogy with equation (5), the integral cross-section is written as

$$\sigma_R = \int \left(\frac{d\sigma}{dE'_T}\right) dE'_T \quad \text{for } 0 < E'_T < E \tag{6}$$

where E is the total energy available to products. Similarly, the differential cross-section is a function of the reagent collision energy. The *differential (product energy) excitation function* $\sigma_R(E_T, E'_T)$ measures the collision energy dependence for scattering into a given final translational energy. Its determination generally requires the use of time-of-flight techniques.

It would be desirable to measure the differential cross-section with full resolution of final quantum states (e', v', j', m') and full specification of initial quantum states (E_T, e, v, j, m); e.g. one would like to measure the quantity

$$d^2\sigma(E_T, e, v, j, m \rightarrow e', v', j', m', \theta)/d^2\omega,$$

where e, v, and j specify the electronic, vibrational and rotational states and m is the magnetic quantum number of the angular momentum vector. Typically, electronic channels are rather obvious and magnetic sub-levels are not resolved in the experiment, so the above differential cross-section is degraded to

$$d^2\sigma(E_T, v, j \rightarrow v', j', \theta)/d^2\omega. \tag{7}$$

Such a differential cross-section has seldom been determined because it implies the measurement of angular scattering for well-defined reagent and product quantum states at a given, well-defined collision energy. As will be shown later in this paper, this measurement could be carried out by the use of optical techniques under crossed-beam conditions, through the high-resolution analysis of laser-induced fluorescence profiles (Kinsey 1977, L'Hermite *et al.* 1990, Girard *et al.* 1991). More often, the use of optical techniques leads to the determination of integral cross-sections for a given set of initial and final states. That is, one measures the quantity

$$\sigma(E_T, v, j \rightarrow v', j') = \int (d^2\sigma(E_T, v, j \rightarrow v', j', \theta)/d^2\omega)\, d^2\omega \tag{8}$$

which is called the *partial cross-section*. Currently, state-selected cross-sections for production of AB products are obtained by summation over all v' and j' product channels

$$\sigma(E_T, v, j) = \Sigma_{v'j'} \sigma(E_T, v, j \rightarrow v', j'). \tag{9}$$

The normalized product state distribution for reaction with state-selected reagents is then defined by

$$P(E_T, v, j \rightarrow v', j') = \sigma(E_T, v, j \rightarrow v', j')/\sigma(E_T, v, j). \tag{10}$$

In the case where beam-gas and cross-beam experiments are carried out without state selection of the reagents, total reaction cross-sections or product state distributions represent an average—thermal, for example—of the above partial cross-sections.

Thus reaction cross-sections can be singly-, doubly-, triply-differential etc.,

depending upon the degree of sophistication of the experimental set-up, the preparation of the reagents, or the characterization of the products. Indeed, they could also be differential with respect to the reagent's angle of approach in c.m. or with respect to the impact parameter, all information which is essential to understand the stereodynamics of the reaction. The first approach has been realized by the use of various technical means (Levine and Bernstein 1987), whereas the second is still out of reach, although it has been possible to evaluate the influence of the impact parameter through the determination of the opacity function in kinematically-constrained reactions (Noda *et al.* 1986). Finally, it might be worthwhile to point out that even the most advanced theoretical calculations are generally not able to reproduce all of these details but only part of them, e.g. fine structure or vibrational excitation of atomic/molecular reagents, vibrational and rotational product distributions, or stereospecificity. In the present status of the theory, this is mainly due to the complexity and duration of the calculations.

2.2. *Vector correlation*

Since the early days of reaction dynamics the vectorial character of the elementary chemical reaction has been well-recognized. In this view not only scalar quantities such as collision energy or total reaction cross-section are important in governing the reactive collision. Vectorial properties such as the reagent's orientation, orbital or molecular alignment can also significantly influence the outcome of the elementary chemical reaction.

For the $A + BC \rightarrow AB + C$ reaction, the partition of the total angular momentum $\mathbf{J}$, between the initial and final momentum of the colliding particles $\mathbf{I}$, $\mathbf{I}'$ and rotational momentum of the reactant and product molecules $\mathbf{j}$, $\mathbf{j}'$, has been shown to be very useful in the diagnosis of the reaction dynamics. The main problem is that even if one collides two molecular beams with well-defined speeds and directions one cannot select the impact parameter and its azimuthal orientation about the initial relative velocity vector. A currently popular way to circumvent this lack of resolution is to use vector correlations, particularly in laser studies, photofragmentation dynamics, and, in general, in the so-called 'dynamical stereochemistry' field. One of the most commonly used correlations is that between the product rotation angular momentum and the initial and final relative velocity vectors.

Figure 1 shows a pictorial representation of the so-called 'two-vector' correlation, both in photodissociation (half collisions) and in atom-exchange reactions (full collisions). The important point to consider is that photodissociation is an anisotropic process in which the polarization of the electric field, ε_p, of the photolysis laser defines a direction with respect to which the vector describing both products and parent molecule can be correlated. In consequence, one can measure and analyze the correlation between the parent transition dipole moment $\boldsymbol{\mu}$ and the recoil photofragment velocity vector, i.e. the $\boldsymbol{\mu}\cdot\mathbf{v}$ correlation. Thus the angular distribution of the photofragments $I(\theta)$ can be described in the form (Zare, 1972)

$$I(\theta) \propto \frac{1}{4\pi}[1 + \beta P_2(\cos\theta)] \tag{11}$$

for a non-degenerate transition, where $P_2(\cos\theta)$ is the second Legendre polynomial, β the so-called 'anisotropy' parameter, which governs the shape of the fragment angular distribution whose value is determined by the nature of the transition and the time

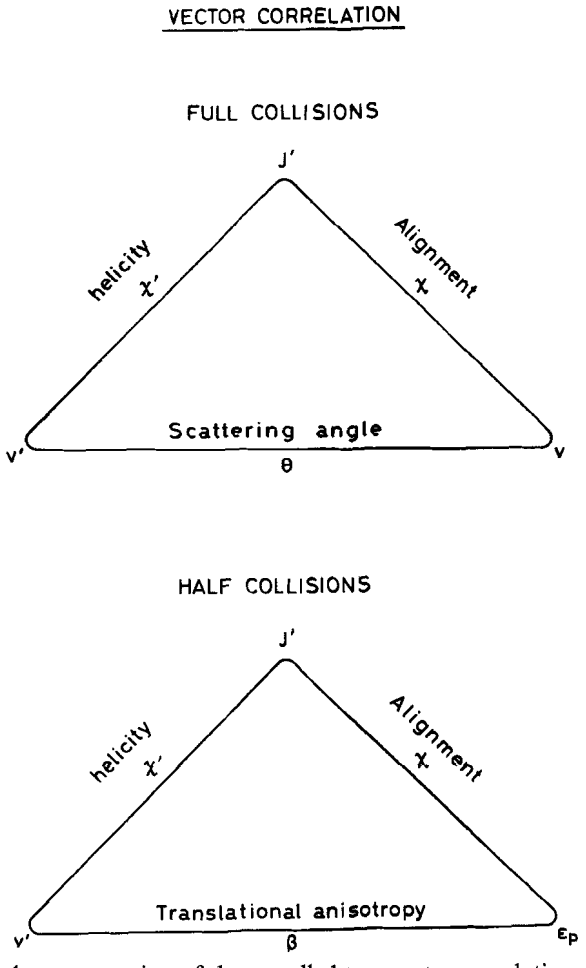

Figure 1. Pictorial representation of the so-called two-vector correlation; top: full collision; bottom; half collision; photofragmentation.

scale of the photodissociation, among other factors. In the above equation, θ is the angle between the space fixed axis and the target fixed axis, i.e. typically between the detector direction and the electric field of the laser polarization.

In a full collision experiment, e.g. crossed-beam, beam-gas, or gas cell arrangement, the reference axis is the relative velocity vector so the vector correlation (top of figure 1) is conceptually identical to that of photodissociation once this change is taken into account. In fact, the conventional product angular distribution of a crossed-beam experiment constitutes a good example of a two-vector correlation, e.g. the $\mathbf{v}\cdot\mathbf{v}'$ correlation.

Let us consider the simplest kind of angular correlation, the direction–direction correlation between a vector **X** and a reference axis **Z** of cylindrical symmetry. The azimuthal angle ϕ of **X** about **Z** is thus uniformly distributed, and the polar angle θ between **X** and **Z** is the observable quantity specifying the directional correlation. The probability distribution for θ is typically represented by an expansion in Legendre polynomials

$$n(\theta) = 1 + a_1 P_1(\cos\theta) + a_2 P_2(\cos\theta) + \ldots = \Sigma a_i P_i(\cos\theta),$$

and hence the anisotropy is characterized by the Legendre moments

$$a_n = (2n+1) < P_n(\cos\theta) > (\text{for } n \geqslant 1)$$

which are averages of the polynomials over the $n(\theta)$ distribution.

The anisotropy of the vector **X** may exhibit either alignment or orientation. These terms specify whether or not the distribution of **X** is symmetric with respect to a plane perpendicular to the **Z** axis. If reflection in this plane leaves the distribution unchanged, **v** is aligned but not oriented; only even-order Legendre moments will then be non-zero. If reflection does change the distribution, **X** is oriented; odd-order moments then are non-zero and measure the sense and size of the orientation.

For a state **J** of the rotational angular momentum there are in general $2J+1$ moments in the expansions which are typically denoted by $A_q^{(k)}$. Under conditions where axial symmetry is preserved, only the $A_0^{(k)}$ moments are non-zero. The majority of experiments restrict the determinable moments to no more than the fourth rank moment. Typically, for unpolarized or linearly polarized light the even moments $A_0^{(0)}$ and $A_0^{(2)}$ are non-vanishing; for circularly polarized light the odd moment $A_0^{(1)}$ is non-zero. Once these moments are properly normalized they can be written as

$$\begin{aligned} &\text{Population: } A_0^{(0)} = 1 \\ &\text{Orientation: } A_0^{(1)} = \langle (J/J_z/\mathbf{J}/J) \rangle = \langle P_1(J\cdot Z) \rangle \\ &\text{Quadruple alignment: } A_0^{(2)} = \langle (J/(3J_z^2 - \mathbf{J}^2)/\mathbf{J}^2/J) \rangle = 2\langle P_2(J\cdot Z) \rangle \end{aligned} \tag{12}$$

where the classical limit has been written in terms of P_n, the Legendre polynomial. As can be seen, orientation refers to odd spatial moments of the fragment angular momentum vector distribution. For a diatomic fragment, orientation is equivalent to the existence of a preferred sense of rotation (either clockwise or counterclockwise); on the other hand, alignment is equivalent to the existence of a preferred plane of rotation.

A positive quadrupole alignment, $A_0^{(2)}$, indicates a parallel alignment of **J** along the Z axis; a negative value indicates a perpendicular alignment. Experimentally orientation and/or alignment of a photofragment **J** vector can be manifest as a non-isotropic response to an interrogating probe laser, or as polarization of spontaneous emission.

In photofragmentation dynamics experiments the rotational alignment is obtained by analysis of laser polarized broad band spectra. Thus, the laser-induced fluorescence (LIF) of a fragment, I, due to a photodissociation process is given by (Greene and Zare 1982)

$$I \sim P(J) B\{q_0 + q_2 A_0^{(2)}\} \tag{13}$$

where $P(J)$ is the fragment population in the state J, B the transition probability, q_0 and q_2 are parameters that depend on the transition and on the experimental geometry, and $A_0^{(2)}$ is the rotational alignment parameter which measures the $\boldsymbol{\mu}\cdot\mathbf{J}$ correlation, i.e. the correlation between the transition dipole moment $\boldsymbol{\mu}$ and the fragment angular momentum **J**. Typically, when using broad band polarization spectroscopy, $A_0^{(2)}$ is determined from the LIF intensities at different geometries via equation (13).

The other correlations $\boldsymbol{\mu}\cdot\mathbf{v}$, $\mathbf{v}\cdot\mathbf{J}$ and $\boldsymbol{\mu}\cdot\mathbf{v}\cdot\mathbf{j}$ are extracted using narrow band and sub-Doppler polarization spectroscopy, e.g. from the analysis of the Doppler profiles at different geometries. The reader is addressed to the usual vector correlation treatments of Greene and Zare (1982) and Dixon (1986) for a full discussion of this topic.

In chemiluminescent reactions a great deal of information about the stereodynamics of the reaction can be gained by measuring the polarization of the chemiluminescence emission. The degree of polarization can be directly related to the alignment of the rotational angular momentum of the emitter for some electronic transitions (see §4.4).

2.2.1. *A prototypical case: The heavy plus heavy–light reaction*

In the study of light atom exchange reactions the so-called 'heavy plus heavy–light' reaction constitutes one of the best examples in which important kinematical factors control the scalar and vectorial properties of the elementary chemical process. From the scalar point of view it is well-known that useful information about the reaction cross-section, including its collision energy dependence, can be gained by measuring the rotational energy distribution of the products. On the other hand, from the stereodynamical viewpoint the study of these kinematically-constrained reactions has often revealed a strong polarization of the product rotational angular momentum. This condition holds as long as the initial reactant rotational angular momentum is small, which is usually true under molecular beam conditions. In addition, because the orbital angular momentum of the reaction product is so small, a large fraction of the initial orbital angular momentum **L** is transformed into rotational angular momentum of the product molecule **j**, e.g. $\mathbf{L} \simeq \mathbf{j}$.

In general for the $A + BC \rightarrow AB + C$ reaction, when the departing atom is not too light, the angular momenta correlation adopts the form (Levine and Bernstein 1987)

$$\mathbf{j} = \mathbf{L}\sin^2\beta + \mathbf{j}\cos^2\beta + \mathbf{d}\cos^2\beta \tag{14a}$$

$$\mathbf{L} = \mathbf{L}\cos^2\beta + \mathbf{j}\sin^2\beta - \mathbf{d}\cos^2\beta \tag{14b}$$

where **d** is a vector depending on the reaction dynamics and is given by $\mathbf{d} = \tan\beta\,(Q_1 \times \dot{Q}_2 + Q_2 \times \dot{Q}_1)$, Q_1 and Q_2 being the A + BC mass-weighted coordinates. In the above expressions β is the so-called 'skew angle' so that

$$\cos^2\beta = m_A m_C/(m_B + m_C)(m_A + m_B).$$

Of course, for a heavy plus heavy–light system $\cos^2\beta \rightarrow 0$. Therefore:

$$\mathbf{j} \simeq \mathbf{L} \tag{15a}$$

$$\mathbf{L} \simeq \mathbf{j} \tag{15b}$$

which represents the kinematic limit of complete transfer of reagent orbital (rotational) angular momentum into product rotational (orbital) angular momentum. Whereas there are many examples of the $(\mathbf{j}\cdot\mathbf{L})$ correlation from extensive analysis of product polarization data, little is known about the other vector correlations, e.g. the complete transfer of **j** into **L** (Albertí *et al.* 1995).

2.3. *Experimental techniques*

As said before, the 'ideal' experiment does not yet exist. One is faced with three main types of experiments to ensure single-collision conditions. Their contrasted characteristics offer a wide field of applications.

2.3.1. *Gas cell experiments*

In this case, the reagents are present in the cell but do not react unless a well-defined excitation initiates the reaction. It is generally realized by use of short laser pulses, the first pulse to compensate for the endoergiticity of the reaction and a second pulse to

probe the reaction products ('pump–probe' technique, Breckenridge and Umemoto (1981, 1984)). Reagents are kept at low pressure, and the time delay between the two laser pulses is adjusted to avoid secondary collisions which would thermalize the sample. Velocity distributions are typically Maxwell–Boltzmann, without privileged direction or magnitude. This means that there is no way of determining angular or kinetic distributions and that partial cross-sections are thermally averaged. Actually, for an $A + BC \rightarrow AB + C$ reaction it is possible to determine the rate of formation of C products by analogy with (1)

$$\frac{d[C]}{dt} = \sigma_R V_R [A][BC] = \frac{[C]}{\tau} \tag{16}$$

where τ is the time delay between the two laser pulses. In a different version of the experiment, the first laser pulse is used to photolyse a molecular compound AA′ whose component A is then able to react with the BC primary reagent (Hering *et al.* 1980, Scherer *et al.* 1987). In this case, the relative velocity of the reagents can be changed by varying the wavelength of the photolysis laser (Tsukiyama *et al.* 1980, van der Zande *et al.* 1991). It is also possible to obtain information about the real time evolution of the reactive collision, the first laser pulse being used to determine the time $t = 0$ and the second one to monitor the yield of AB products versus time.

Recently, a novel technique has been developed in which a chemiluminescent reaction is induced via the absorption of a laser pulse by an atomic reagent; the subsequent chemiluminescence is dispersed to obtain information about product states. The time profile measurement of both reagent and product decays allows for the determination of specific rate constants in absolute values (Autrobus *et al.* 1995).

2.3.2. *Beam-gas experiments*

In this case a beam of particles A enters a low pressure vapour of molecules BC and the reaction occurs in the common volume. Due to the axial symmetry of the arrangement, the collision axis can be roughly defined between two extremes of magnitude and direction, hence the possibility of obtaining some crude information about angular scattering. The experiment is rather well-adapted to absolute measurements of detailed rate constants, in particular when the 'depletion' technique is used (Dagdigian and Campbell 1987). A first cw laser beam is used to decrease the population of a given atomic level in the beam, and a second one is used to monitor the product population through laser-induced fluorescence, for example. Typically in this experiment one obtains partial reaction cross-sections according to (9).

As is well-known, molecular photodissociation of simple systems generates velocity-aligned atomic fragments that can be referenced with respect to the laboratory frame when the dissociation process is fast enough. If these fragments have a large velocity, their subsequent interaction with unreacted molecules look similar to 'super-thermal beam-gas' collisions with stationary target molecules. In this manner, it is possible to gain insight into the dynamics and stereodynamics of simple reactions under bulk conditions (Brouard *et al.* 1991, 1993).

2.3.3. *Crossed-beam experiments*

Crossed-beam experiments usually offer the clearest experimental conditions. Due to the low density of the particles, typically between 10^9 and 10^{12} molecules cm^{-3} (Campargue *et al.* 1981, Miller 1988), and to the magnitude of reactive cross-sections, the probability of observing single reactive collisions is small and is negligible for

secondary reactive collisions. Since under usual conditions reagent velocities are generally well-defined—and can be varied in direction and magnitude—the experiment is well-adapted to differential cross-section measurements for angular scattering and collision energy dependence. From the product flux-velocity angle distributions measured in the laboratory frame and transformed into the c.m. system, one usually gets the triply-differential cross-section $d^3\sigma(\theta, w')/d^2\omega\, dw'$, where w' is the product recoil velocity in c.m. (González Ureña 1987). This triply-differential cross-section is a sum over discrete contributions from all internal states of the reaction products, meaning that energy-averaging smears out the quantum nature of these internal states. The problem is solved if, in addition, high-resolution laser techniques are applied to fully characterize the state of reaction products. Under these conditions, one measures the corresponding partial cross-sections, hence a more complete description of the chemical process 'before' and 'after' the reactive collision. Such an experiment is also well-suited to measurements with aligned/oriented atomic/molecular reagents, generally speaking, for all measurements which imply some anisotropy of reagents or reaction products. As said before, however, there is no way to control the impact parameter and thus follow the real time evolution of the reactive system by the use of short laser pulses.

3. Laser characterization of reaction products

The objective of this section is to show how, by the use of standard laser techniques, it is possible to characterize the state of reaction products and to obtain detailed information about the collision dynamics. It is assumed here that the chemical reaction yields atomic/molecular products in their ground electronic state. Essentially, the aim is to obtain differential angular and partial cross-sections through expressions (7) and (9), where the reagent state and the collision energy are not specified. This means that one has to determine the angular distributions in c.m. for all product quantum states in the first case and the various vibrational and rotational distributions in the second case.

Three principal laser techniques have been involved in this enterprise: laser-induced fluorescence (LIF), multiphoton ionization (MPI) and coherent anti-Stokes Raman spectroscopy (CARS). Their common principle is detection of reaction products once they have been excited by absorption of laser light. The three techniques differ by the method of detection: in the case of LIF, by direct collection of their fluorescent light emission, in the case of MPI, by ionization from the excited states, and in the case of CARS, by induction and detection of Raman optical transitions. In this manner, one takes advantage of the high spectral resolution of the laser and probes all the product quantum states populated by the reaction just by tuning the laser frequency. LIF is a single photon technique which can be used with pulsed as well as with cw lasers; it is the only technique which has been used to carry out angular analyses in crossed-beam experiments, and it is by far the most popular due to its greater flexibility and its ability to yield quantitative results. The two other techniques are multiphoton, generally implying the use of high intensity pulsed lasers; MPI is probably a more universal technique due to the simplicity and high efficiency of ion collection.

3.1. *Laser-induced fluorescence*

The LIF technique of detection involves a tunable laser beam which excites the sample when its frequency is tuned to an absorption transition. The subsequent fluorescent light emission is detected and recorded versus laser frequency, yielding the

'excitation spectrum' $E(v)$, which is equivalent to the usual absorption spectrum $\alpha(v)$. However, the LIF technique offers several advantages with respect to absorption, essentially, higher sensitivity and higher resolution. If photon counting techniques are used $E(v)$ and $\alpha(v)$ are connected by the simple relation

$$E(v) = \frac{Z(v)}{\Phi(v)} = \alpha(v)\,\Delta V\,\delta\eta \tag{17}$$

where $Z(v)$ is the photon count rate at frequency v, $\Phi(v)$ the incident photon flux, ΔV the cross volume, δ the collection efficiency of the optics, and η the quantum efficiency of the photomultiplier. Since fluorescence is emitted isotropically over a whole set of transitions at various frequencies, the light background can be reduced to the photon noise of the detector, leading to a striking increase in sensitivity relative to usual absorption, up to a factor of 10^8 when optimal conditions are fulfilled (Demtröder 1992). $E(v)$ is not distorted with respect to $\alpha(v)$ if the width of the apparatus function is small with respect to other sources of broadening. If the sample is a well-collimated atomic/molecular beam, it is possible to eliminate Doppler broadening just by crossing the two beams at a right angle. Then the spectral width of LIF profiles is mainly determined by the width of the laser oscillation and by the natural width of the transition. This width can be reduced to less than 10^{-8} cm^{-1} if tunable cw lasers are used (Jacquinot 1976). Lastly, it is possible to detect the polarization of the fluorescence emission.

Application to high-resolution atomic/molecular spectroscopy has been studied in great details. For comprehensive and quantitative analyses, the reader is addressed to basic articles (Hefter and Bergmann 1988, Demtröder 1992). Application to crossed-beam experiments reveals particular aspects:

(i) Reaction products are probed only once. Indeed, as the fluorescence emission is performed over a whole set of transitions, the branching ratio toward the initial level is small ('open system'), hence there exists a small probability of repopulating it, a situation which is worsened by the absence of relaxation processes.

(ii) For low laser energy density, the magnitude of the signal is proportional to the number density of absorbing molecules, but a saturation of the response readily occurs with energy density, even with the modest power provided by cw single mode tunable lasers.

(iii) The width of fluorescence profiles is determined by the Doppler shift associated with the recoil velocity of absorbing molecules. Their shape is determined by the differential (angular) cross-section and by geometrical factors associated with the laser beam/collision axis geometrical arrangement.

Under specific conditions which are described in the following, these properties allow for the measurement of partial and differential cross-sections, for each product quantum state.

3.1.1. *Total cross-section measurements*

3.1.1.1. *Absolute cross-section measurements.* Absolute cross-sections are measured by the application of (1), where the main problem is the determination of the flux of reaction products, (dN_{AB}/dt) or, more precisely, of the partial flux to a given quantum

state. The first problem which arises is to determine if LIF leads to flux or to density measurements. Generally speaking, the overall probability $D(v)$ of detecting a product molecule with velocity v in the laboratory frame can be expressed in the form

$$D(v) = P(\rho, A, v)\,\delta\eta(\Omega/4\pi) \tag{18}$$

where the probability $P(\rho, A, v)$ for a molecule in a given rovibrational level of absorbing one photon and re-emitting another (generally at a different frequency) is a function of the laser energy density ρ, the relevant transition probabilities A, and the velocity v. $\delta\eta$ represents the efficiency of light collection and detection, and Ω is the solid angle of fluorescence collection. The fluorescence signal is obtained by averaging over the velocity distribution $g(v)$ of the product molecules

$$S = n \int D(v)\, v g(v)\, \mathrm{d}v \tag{19}$$

where n is the particle density. For low ρ, $P(\rho, A, v)$ is proportional to the transit time inside the cross volume, $(1/v)$, and S is proportional to n. For high ρ, each molecule is able to absorb one photon, $P(\rho, A, v)$ becomes independent of v, and S is proportional to the flux $n \langle v \rangle$.

Generally speaking, the fluorescence signal for excitation from a level j to an excited one j' and subsequent fluorescence to j'' is given by the Breit formula

$$S(j, j', j'') = C(n_j/(2j+1))\, H_{jj'} H_{j',j''} R_{jj',j''} \tag{20}$$

where the proportionality constant C includes such factors as $\rho, \Omega, \delta, \eta$, and dipole transition moments. n_j is the population density in level j, summed over all magnetic quantum numbers m. The H coefficients stand for Höln–London factors for absorption and emission. R is an angular factor which depends upon the geometry of detection with regard to light polarization. Under usual conditions of $(v,j) \rightarrow (v',j')$ absorption and $(v',j') \rightarrow (v'',j'')$ fluorescence, relation (20) becomes

$$S(v,j) = C'(n_j/(2j+1))\, q_{vv'} \tau_{v'} \Sigma\, q_{v'v''} \nu^4_{v'v''} S(\nu_{v'v''})\, R_{jj'j''} \tag{21}$$

where the sum is performed over v'' (Bernstein 1982). The q stand for Franck–Condon factors, $\tau_{v'}$ is the lifetime of the upper level, v', and $S(\nu_{v'v''})$ is the detector efficiency at $\nu_{v'v''}$. If individual rotational lines are not resolved in the spectrum, vibrational populations can be estimated, assuming a given rotational distribution, for example, a 'prior', statistical distribution (Levine and Bernstein 1987); simulated spectra are then adjusted to the experimental one by the use of a fitting procedure. Equation (21) shows that to convert fluorescence intensities into product populations it is required that the parameters of the set-up are controlled and that the kinetics of absorption–emission and the relevant spectroscopic data are known.

It is outside the scope of this paper to enter into details about the long tramping leading to the LIF signal, as calculated by Hefter and Bergmann (1988), for the most general case, by solving the appropriate system of rate equations which governs the evolution of state populations. It is shown that the photon count rate corresponding to product molecules in a given quantum state is determined by 'molecular' parameters, including transition probabilities and line-strengths, by 'experimental' parameters involving collection and quantum efficiencies of detection optics and also by factors which characterize the detailed interaction between the reaction products and the laser field: the interaction time, the energy density of the laser, and the polarization and coherence time. In the case of weak excitation probability between

rotational levels i and f, isotropic population of magnetic sub-levels in level i, and for particular polarization axis/detector axis geometrical arrangements the photon count rate $Z(i)$ reduces to (see expression 9.107 in Hefter and Bergmann (1988)

$$Z(i) = (1/3)\, n(i)\, (\mu/h)^2\, F_{if}\, S_{if}\, E_0^2\, \Delta t (F/\gamma)\, \delta\eta\, (\Omega/4\pi). \tag{22}$$

Here $n(i)$ is the population density in the rotational level i which is probed, μ is the transition dipole moment, F_{if} is the Franck–Condon factor, S_{if} is the line strength, E_0 is the field amplitude, and Δt is the interaction time. γ is the absorption width and F is a width related to the spectral width γ_L of the laser oscillation. This expression shows in particular that the response is proportional to the intensity of the laser field and to the transit time. Generally speaking, however, there is a direct correspondence between $Z(i)$ and $n(i)$ only in the particular cases where the non-isotropic character of the fluorescence emission induced by light polarization can be neglected or cancelled.

Saturation effects observed when using pulsed lasers have been treated in detail (Hefter and Bergmann 1988, Altkorn and Zare 1984). In this case, the interaction time is determined by the coherence time of the laser, and the LIF signal is proportional to the particle density $n(i)$ only if the lifetime of the upper level is short enough. The density $n(i)$ can be calculated through the solution of the usual rate equations involving level populations, transition probabilities, and the laser energy density. In any case, due to the magnitude of γ_L, profile analyses are not feasible.

Saturation effects may also arise when using cw single-mode lasers (Billy *et al.* 1987, 1990). If the laser field is strong enough, rapid oscillations are forced between the two levels of the transition because the coherence time of the laser is long with respect to the interaction time—now the transit time Δt—and the lifetime τ of the upper level. Their frequency at resonance is described by the Raby formula (at resonance)

$$f = E_0(\pi/8)\, h^{-1} \langle X|\mu|A\rangle \langle v'|v''\rangle. \tag{23}$$

In this expression, E_0 is the field amplitude, $\langle X|\mu|A\rangle$ is the transition dipole moment, $\langle v'|v''\rangle$ is the Franck–Condon factor and the $(\pi/8)$ factor arises from the overlapping of the angular part of the two wavefunctions. With normal energy densities provided by cw lasers and for large values of the dipole moment, the period $T = 1/f$ of these oscillations is easily shorter than Δt, so that many forced oscillations take place during the interaction time. In addition to level populations, one has then to introduce optical coherences between the two levels of the transition to solve the Schrödinger equation and to obtain the evolution of the populations ('coherent saturation regime'). When particular conditions are fulfilled, $T \ll \Delta t$ and $T^2 \ll \tau \Delta t$, the LIF signal becomes proportional to E_0, not to E_0^2, hence saturation is observed with laser intensity. The interaction between molecules at rest and the laser field is conveniently described by a Lorentzian whose width is equal to $\Delta\nu_R = f(\Delta t/\tau)^{1/2}$ and whose intensity at resonance provides the efficiency of the absorption process (Girard 1987). Currently, because reactive collisions occur inside the collision volume at various places with respect to the probe beam, one has to estimate the actual, effective transit time (L'Hermite *et al.* 1991).

This technique has seldom been applied to the measurement of absolute cross-sections. In addition to dealing with the difficulties inherent to crossed-beam experiments (González Ureña and Vetter 1993, 1995), it requires the use of single-mode tunable lasers to determine the area of fluorescence profiles, the control of various experimental and physical parameters among which the spectral and spatial energy density of the laser beam plays a major role, and finally, the knowledge of

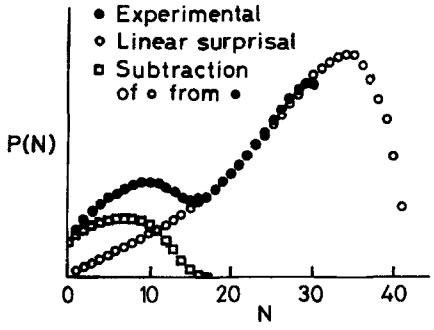

Figure 2. Nascent rotational state distribution of MgH $X\,^2\Sigma^+(v'' = 0)$ (filled circles). The 'prior' statistical distribution is shown for comparison (open circles). The difference between the two previous distributions (open squares) shows the component at low values of the rotational quantum number (from Breckenridge and Umemoto (1984)).

relevant molecular parameters. Moreover, it often requires the prior determination of specific characteristics of the reaction under study, for instance the transit time, which is itself a function of the product recoil energy. To our knowledge it was first applied to the crossed-beam study of the $Cs(7p\,^2P) + H_2 \rightarrow CsH + H$ photochemical reaction, where a cw single-mode tunable dye laser was first used to excite caesium atoms toward the $7p\,^2P$ state and a second cw single-mode tunable dye laser was used to record laser-induced fluorescence profiles under coherent saturation conditions through photon counting techniques (L'Hermite *et al.* 1990, 1991). For this reaction, which proceeds through a non-adiabatic harpooning mechanism (Gadéa *et al.* 1986), it was possible to give absolute values for partial and total reaction cross-sections associated with the two fine structure levels of caesium, and so to show the influence of spin–orbit coupling on the reactivity of caesium (Gadéa and Durup 1987, Gadéa *et al.* 1988). Although affected by large error bars, these measurements allowed for comparison of the reactive cross-sections under study with the inelastic cross-sections related to underlying quenching potential energy surfaces associated with the $6s\,^2S$, $6p\,^2P$, $5d\,^2D$ and $7s\,^2S$ states of caesium (L'Hermite *et al.* 1991).

3.1.1.2. *Relative cross-section measurements.* Relative measurements are of course much easier, as a number of molecular and experimental parameters disappear when directly comparing the signals related to two close product states. For example, for non-saturated 'pump' transitions, the LIF signals corresponding to two rotational levels within the same vibrational state are simply related by

$$\frac{Z(1)}{Z(2)} = \left[\frac{n(1)}{n(2)}\right]\left[\frac{S(1 \rightarrow f_1)}{S(2 \rightarrow f_2)}\right]. \tag{24}$$

By the use of this technique, one normally determines the rotational and vibrational distributions of the reaction products according to (20) or (21). Since the pioneering work of Dagdigian and Zare (Cruse *et al.* 1973, Zare 1979), many experiments have been carried out with pulsed and cw lasers, from which a lot of essential information can be deduced. Figure 2 represents, for example, the nascent rotational distribution obtained for the $Mg(3s3p\,^1P_1) + H_2 \rightarrow MgH + H$ reaction in the $X\,^2\Sigma^+$ ($v'' = 0$) level of MgH. The measurements performed in a 'pump–probe' experiment with pulsed lasers indicated two components, at low and high values of the rotational quantum number, corresponding to two reaction mechanisms, abstraction and insertion, respectively

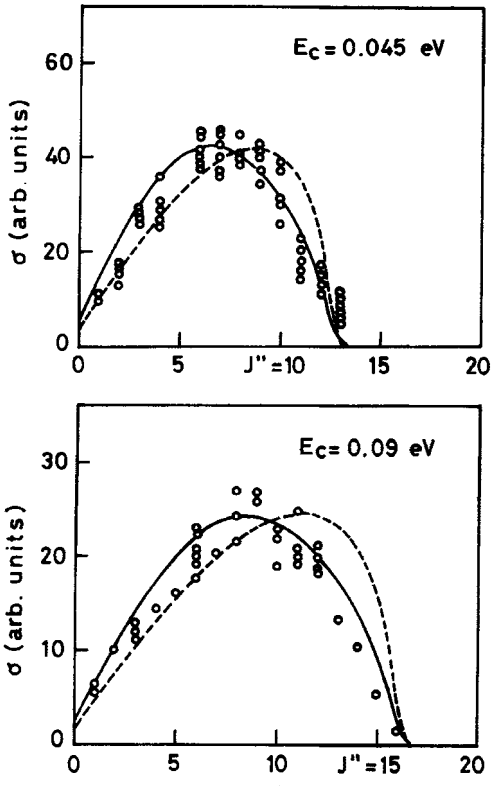

Figure 3. Rotational state distribution of CsHX $^1\Sigma^+(v'' = 0)$ (circles) at two collision energies. The dashed curves represent 'prior' statistical distributions and the full curves the 'prior' with a surprisal parameter equal to 1 (from L'Hermite *et al.* (1991)).

(Breckenridge and Umemoto 1984). Figure 3 represents the rotational distributions observed at two collision energies in the $X^1\Sigma^+$ ($v'' = 0$) level of CsH following the aforementioned photochemical reaction between caesium and hydrogen (L'Hermite *et al.* 1991). These distributions, whose shape is close to 'prior' statistical ones, could be interpreted by quasi-classical trajectory calculations assuming 'direct' and 'indirect' collisions. Direct collisions, associated with large impact parameters, correspond to the classical harpooning mechanism, whereas indirect collisions, associated with small impact parameters, lead to the formation of a $Cs–H_2$ intermediate complex whose lifetime is long enough to allow for charge migrations between the two hydrogen atoms (L'Hermite 1992). Figure 4 represents simulated LIF spectra calculated for the $Si + N_2O \rightarrow SiN + NO$ reaction at various collision energies, where statistical rotational distributions were assumed to take place in the $X^2\Sigma^+$ state of SiN. From the comparison of these spectra with the experimental spectra, it was possible to deduce the reaction endoergiticity and the dissociation energy of the SiN molecule (Naulin *et al.* 1993).

3.1.2. *Differential cross-section measurements*

Under crossed-beam conditions it is usual to consider the Newton diagram, where velocities in the laboratory frame are decomposed into c.m. velocity and velocity in c.m. (figure 5). The usual technique for determining the differential cross-section is to rotate a mass spectrometer around the collision volume and to measure the flux of

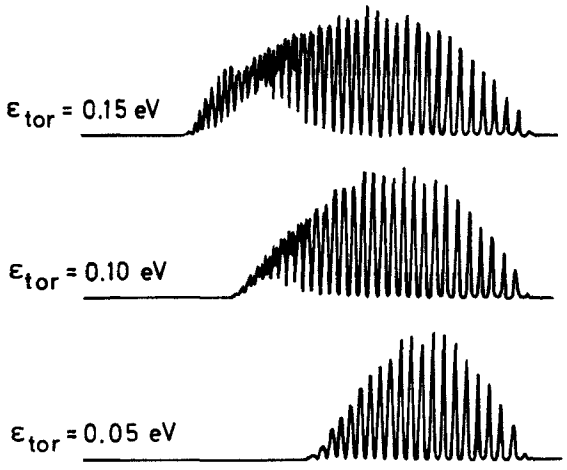

Figure 4. LIF simulated spectra due to the $Si + N_2O \rightarrow SiN + NO$ reaction at three collision energies, actually the total energy available to products. $E_{tot} \simeq 0{\cdot}05$ eV, 0·10 eV and 0·15 eV. The comparison with the spectrum obtained under crossed-beam conditions shows immediately that $E_{tot} \simeq 0{\cdot}10$ eV hence the endoergicity of the reaction and the dissociation energy of SiN (from Naulin *et al.* 1993)).

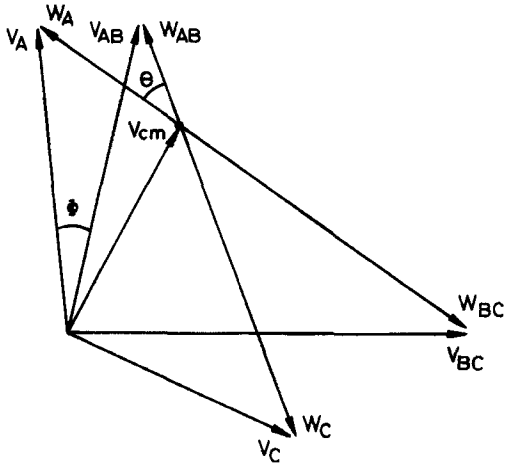

Figure 5. Newton diagram. AB products scatter at the angle θ with respect to the velocity w_A of the incoming atom in c.m.

reaction products versus the angle Φ. $I(\theta)$ or $P(\theta)$ are obtained in c.m. after a complex deconvolution taking initial distributions and dispersions of velocities into account (angle and modulus). On the contrary, as demonstrated many years ago by Kinsey (1977), and recently reviewed by Mestdagh *et al.* (1994), the use of LIF can yield $P(\theta)$ directly in c.m. by analyzing the shape of fluorescence profiles, which are primarily determined by the shape of Doppler profiles due to the product recoil velocity **w** in c.m. One considers the Doppler shift $\delta\nu$ between the resonance absorption frequency ν_0 of the reaction products and their actual absorption frequency ν. $\delta\nu$ is a function of both θ and **w** and also of the geometrical arrangement of the probe laser beam with respect to the collision axis. As expected from §3.1.1, saturation effects should be invoked

here through the profile deformation that they induce (Billy *et al.* 1990). Following L'Hermite *et al.* (1990), one considers the following two beam arrangements.

3.1.2.1. *Parallel arrangement.* In this case, the laser beam axis is adjusted along the collision axis. As it is not perpendicular to the c.m. velocity in general, a constant Doppler shift results which does not change the shape of Doppler profiles but only accounts for the distribution of **w** in c.m. Owing to the axial symmetry of angular scattering with respect to the collision axis, the angle α between **w** and its projection over the laser axis is identical to θ. Accordingly, the following Doppler relation holds for $\delta\nu$

$$\delta\nu = \nu_0\left(\frac{w}{c}\right)\cos\theta, \tag{25}$$

where c is the speed of light. N being the total number of scattering molecules, the number of molecules which scatter between θ and $\theta+\mathrm{d}\theta$ is (see equation (5))

$$\mathrm{d}N = 2\pi N P(\theta)\sin\theta\,\mathrm{d}\theta. \tag{26}$$

From the Doppler relation, these molecules are excited in the frequency interval

$$\mathrm{d}\nu = \nu_0\left(\frac{w}{c}\right)\sin\theta\,\mathrm{d}\theta. \tag{27}$$

The Doppler profile is proportional to the number of product molecules per spectral element

$$D(\nu-\nu_0)\,\alpha\frac{\mathrm{d}N}{\mathrm{d}\nu} = 2\pi N\frac{P(\theta)}{(\nu_0 w/c)}. \tag{28}$$

Accordingly, there is a direct connection between $D(\nu-\nu_0)$ and $P(\theta)$, with the quantity $2\pi\sigma P(\theta)\sin\theta$ representing the fractional contribution $\mathrm{d}\sigma/\mathrm{d}\theta$ for scattering at θ. With this beam arrangement, the angular resolution $\mathrm{d}\nu/\mathrm{d}\theta$ is lowest for θ values around 0 and π. However, it is not suitable for attaining high signal-to-noise ratios, since the adjustment of the laser beam along the collision axis generally yields stray light in the collision chamber; moreover, it depends on the reagent kinetic energy.

3.1.2.2. *Perpendicular arrangement.* In this case, the laser beam axis is perpendicular to the reagent velocities in the laboratory frame and to the collision axis. The relation between $D(\nu-\nu_0)$ and $P(\theta)$ is not direct because θ is now a function of α and the azimuthal angle ϕ between the collision axis and the projection of **w** over the collision plane ($\theta = \arccos(\sin\alpha\cos\phi)$). The same kind of calculation as for the parallel case leads to

$$D(\nu-\nu_0)\,\alpha\frac{\mathrm{d}N}{\mathrm{d}\nu} = -\frac{N}{(\nu_0 w/c)}\int P[\theta(\alpha,\phi)]\,\mathrm{d}\phi. \tag{29}$$

The determination of $P(\theta)$ is then not direct because the products which scatter at θ and at $(\pi-\theta)$ lead to the same absorption frequency in the Doppler profile. In other words, it is not possible to distinguish 'forward' from 'backward' scattering—or their sum. In all cases, the Doppler profile is symmetrical with respect to ν_0, and the angular resolution is lowest for θ values around $\pi/2$. This arrangement is most suitable in crossed-beam experiments as it leads to a minimum of stray light in the collision chambers.

The unambiguous and accurate determination of $P(\theta)$ results from measurements taken from these two arrangements, which appear more complementary than contradictory. It was shown that two different beam arrangements—not necessarily

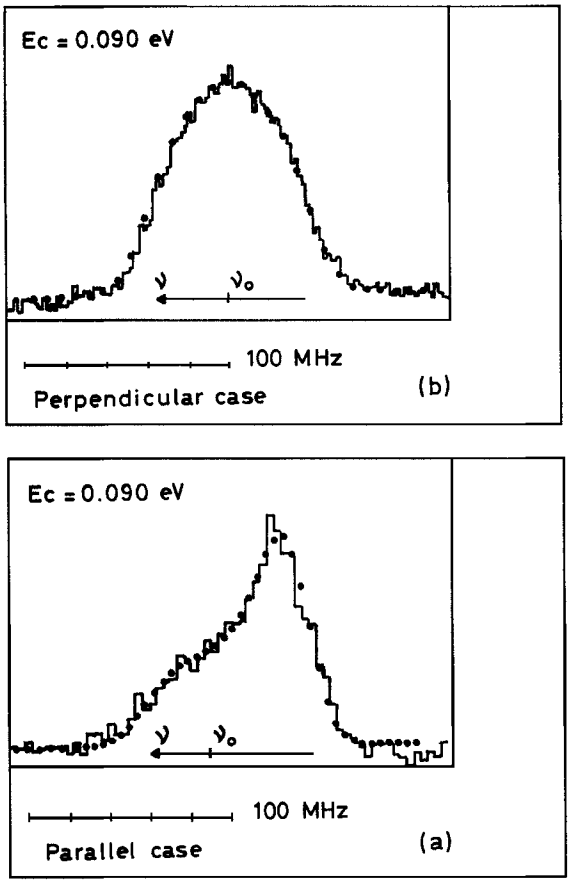

Figure 6. Recorded LIF profiles of CsH $^1\Sigma^+(v'' = 0)$ for $J'' = 11$ with a parallel arrangement (a) and a perpendicular one (b). Dots represent the result of a best fit calculation assuming a forward peaking of products superposed to an isotropic one (from L'Hermite *et al.* (1990)).

parallel or perpendicular—are enough to determine $P(\theta)$ through a deconvolution procedure followed by a numerical inversion method (Serri *et al.* 1981b). This method was applied successfully to inelastic scattering measurements under crossed-beam conditions (Phillips *et al.* 1978, Serri *et al.* 1981a, Moskowitz *et al.* 1984, Smith *et al.* 1984). It was applied for the first time to reaction scattering on the $NO_2 + H \rightarrow NO + OH$ reaction (Murphy *et al.* 1979) and later on the $Cs(7p\,^2P) + H_2 \rightarrow CsH + H$ and $I_2 + F \rightarrow IF + I$ reactions. In the case of caesium and hydrogen, the photochemical reaction is quasi-isoenergetic, so that the kinetic energy available to CsH products is necessarily small, leading to very narrow Doppler profiles (L'Hermite *et al.* 1990). In spite of this difficulty, it could be shown that the differential cross-section presents a pronounced peaking for small θ values superposed to a flat, continuous background for all θ angles. Figure 6 shows the comparison between recorded and calculated fluorescence profiles obtained with parallel and perpendicular arrangements. Following the quasi-classical trajectory calculations performed for this reaction (L'Hermite 1992), the peaking would result from direct collisions with large impact parameters whereas the background would result from indirect collisions with small

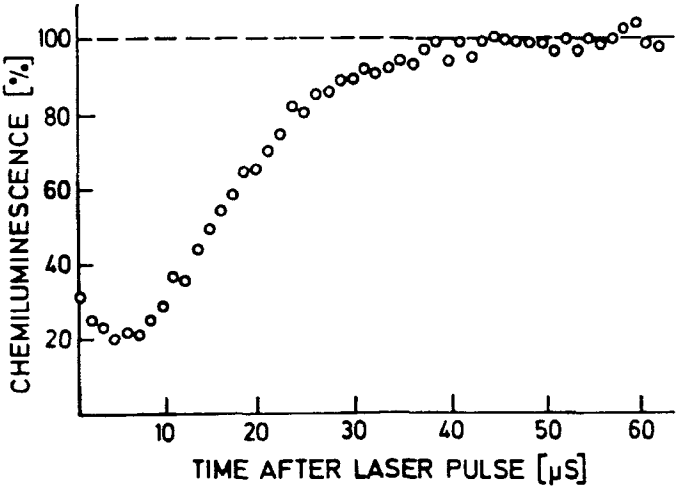

Figure 7. Chemiluminescence signal as a function of time after the laser pulse. The broken lines indicates dc level with laser off (adapted from de Vries *et al.* (1983)).

impact parameters. This shape was shown to vary slightly with reagent kinetic energy but not with the rotational quantum number of CsH. As for the reaction between iodine and fluorine atoms, it was possible to show that the differential cross-section is generally flat at high J values (≈ 150) and peaks preferentially in the forward direction at low J values (Girard *et al.* 1991). To our knowledge, this was the first time that this kind of variation had been observed directly in reactive scattering. The interpretation was based on the assumption of direct collisions and migratory ones but, unfortunately, potential surfaces and collision dynamics could not be calculated for this reaction.

3.1.3. *Reagent and product polarization experiments*

Laser photodissociation can also be used to selectively remove most of the m state distribution of a molecular reagent. Thus, the orientational dependence of the reaction cross-section can be studied. Recently, the orientation dependence on the Xe* + IBr reactions was studied (de Vries *et al.* 1983). Essentially, the reaction of metastable Xe* with IBr to produce XeI* and XeBr* excimers was studied in crossed molecular beams.

Figure 7 shows the excimer emission intensity as a function of time after the laser pulse. The broken line indicates the chemiluminescence intensity with the laser off and the particle beams on. The laser pulse depletes the IBr beam within and just before the Xe* interaction region. Note how the dip in the IBr beam intensity moves through the Xe* beam, the excimer emission decreases to a minimum of about 5 μs, and then increases back to the dc levels as the dip exits to the crossed-beam region. In the experimental arrangement, the laser beam was orthogonal to the particle beams. The light was linearly polarized, and the light plane was rotated using a half-wave plate.

The reaction cross-section was found to be largest when the Xe* approaches parallel to the plane of rotation of the IBr, and smallest when the Xe* approaches perpendicular to the plane of rotation. These results were rationalized by steric effects resulting from the anisotropy of the ionic Xe^+/IBr^- ($^2\Pi$) potential surface, i.e. the first excited state of IBr^-, which is the intermediate state in the formation of XeI*.

3.1.3.1. *Beam-gas studies: bimolecular reaction dynamics in a bulb.* As is well-known,

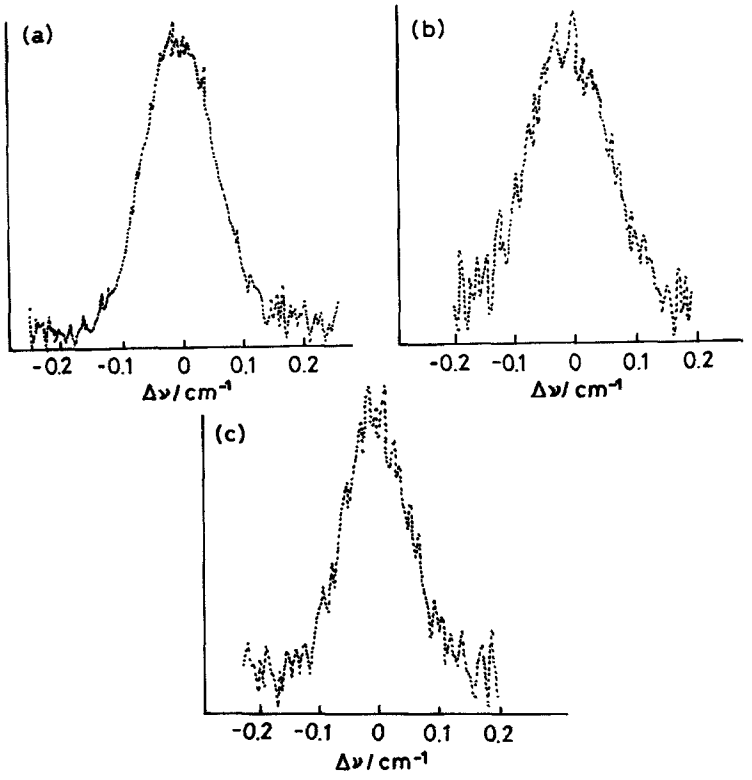

Figure 8. Representative Doppler broadened profiles from (*a*) NO($v' = 16, N'' = 32$) in pump–probe geometry with both laser photolysis and probing electric vector parallel, (*b*) same as for (*a*) but with both electric vectors perpendicular and (*c*) NO($v' = 17$, $N' = 23$) with both laser parallel (adapted from Brouard *et al.* (1992)).

many simple molecular photodissociation systems generate velocity aligned atomic fragments that can be referenced to the laboratory frame when the dissociation is a fast process. If the fragment velocity is very large, subsequent collisions with unreacted molecules in the gas cell closely resemble the 'super-thermal beam-gas' conditions having stationary target molecules. When the nascent bimolecular reaction products are measured under single-collision conditions one can obtain insight into the dynamics and stereodynamics of these so-called 'beam-gas' studies of bimolecular reactions dynamics in a bulk. Indeed, Doppler resolution of the polarized, laser-induced fluorescence spectrum can allow for the determination of both scalar and vectorial product distribution. A typical example of this new technique is the stereodynamical study of the highly exothermic reaction

$$O(^1D) + N_2O \rightarrow NO + NO$$

following the generation of super-thermal velocity aligned $O(^1D)$ atoms via photodissociation of N_2O at 193 nm (Brouard *et al.* 1991).

Figure 8 shows a representative Doppler broadened profile obtained from the $O(^1D) + N_2O \rightarrow NO(v' = 0) + NO(v' = 16, 17)$ reaction. The Doppler profile corresponds to $NO(v' = 16, N' = 32)$ product molecule, whose laboratory velocity distribution is shown in figure 9. In this study by Brouard *et al.* (1992), it was concluded that the wider distribution of $NO(v' = 16, 17)$ velocities primarily reflects

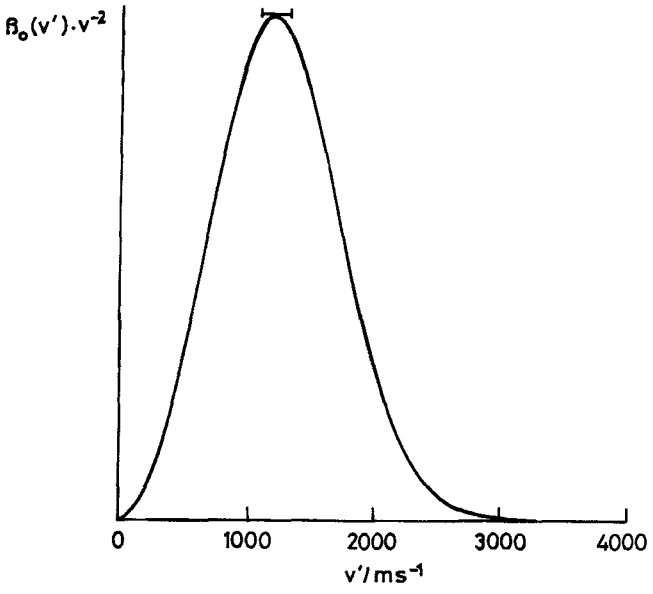

Figure 9. The experimentally determined NO($v' = 16$, $N' = 32$) product lab velocity distribution arising from the photoionization $O(^1D) + N_2O$ reaction (adapted from Brouard *et al.* (1992)).

the range of collision velocities employed in this hot atom (via N_2O photodissociation) reaction. Nevertheless, the analysis of this Doppler resolved, polarized-laser-induced fluorescence led to the conclusion that the above reactive channel proceeds via direct stripping dynamics. In addition the observed product state selective linear and angular momentum disposal was rationalized implying a collinear transition state configuration.

This method constitutes a good example of how high-resolution, polarized laser pump–probe techniques can be complementary to high-resolution crossed molecular beam experiments to unravel the detailed molecular mechanism of reactive and non-reactive collisions.

3.1.3.2. *Product rotational angular momentum alignment by laser-induced fluorescence.* During the atom exchange reaction $A + BC \rightarrow AB + C$ the total angular momentum is conserved $\mathbf{j} + \mathbf{L} = \mathbf{L}' + \mathbf{L}'$. Here $\mathbf{L}$ and $\mathbf{L}'$ are the reagent and product orbital angular momentum and $\mathbf{J}$, $\mathbf{J}'$ the reagent and product rotational angular momentum. In discussing the product angular distributions one deals with one of the simplest kinds of angular correlation (McClelland and Herschbach 1978), the so-called 'direction–direction' correlation between the $\mathbf{v}'$ and $\mathbf{v}$ vectors, e.g. the product velocity versus reagent relative velocity. As was mentioned earlier, another interesting type of two-vector correlation is that of $\mathbf{j}' \cdot \mathbf{v}$ which is described by the θ angle formed between both vectors. For the atom exchange reaction we are considering, in the limit of $\mathbf{L} = \mathbf{j}'$ (pure kinematic limit), only the two even Legendre moments need to be considered, so the angular distribution of $\mathbf{j}'$ is given by $a_0 = 0{\cdot}5$ and $A_2 = a_2/a_0 = -2{\cdot}5 \langle P_2(\mathbf{j}' \cdot \mathbf{v}) \rangle$. In principle, it is possible to obtain $A_2 = a_2/a_0$ and $A_4 = a_4/a_0$ by performing four laser-induced fluorescence polarization measurements. For a parallel type transition,

Table 1. Alignment parameters $\langle P_2(\mathbf{J}\cdot\mathbf{v})\rangle$ for several reactions.

Reaction	$\langle P_2(\mathbf{J}\cdot\mathbf{v})\rangle$	Method	Ref.
$Sr+CH_3Br \rightarrow SrBr+CH_3$	$-0{\cdot}323$	LIF	Li *et al.* (1994)
$Sr+C_2H_5Br \rightarrow SrBr+C_2H_5$	$-0{\cdot}235$	LIF	Li *et al.* (1994)
$Sr+C_3H_7Br \rightarrow SrBr+C_3H_7$	$-0{\cdot}195$	LIF	Li *et al.* (1994)
$Ca(^1D_2)+HBr \rightarrow CaBr(B)+H$	$-0{\cdot}39\pm0{\cdot}012$	Chem.	Garay *et al.* (1995)
$Ca(^1D_2)+HCl \rightarrow CaCl(B)+H(E_T=0{\cdot}1\text{ eV})$	$-0{\cdot}41\pm0{\cdot}02$	Chem.	Menéndez *et al.* (1993)
$Ca(^1D_2)+HCl \rightarrow CaCl(B)+H(E_T=0{\cdot}17\text{ eV})$	$-0{\cdot}44\pm0{\cdot}02$	Chem.	Prisant *et al.* (1981)

i.e. the one for which the transition moment lies along the internuclear axis, and under the simplified beam-gas conditions, it can be shown that

$$A_2 = 5/2\frac{-3/4\,I_{zz}-I_{zx}+2I_{yx}}{3/8\,I_{zz}+I_{zx}+I_{yx}}$$
$$A_4 = 9\frac{-9/4\,I_{zz}-4I_{zx}+I_{yx}}{3/8\,I_{zz}+I_{zx}+I_{yx}} \qquad (30)$$

in which the direction of the beam, laser and detection are defined as the z, y and x axis, respectively.

Table 1 shows $\langle P_2(\mathbf{j}'\cdot\mathbf{v})\rangle$ values for the Sr+RBr reaction as a function of the radical group, being the rest of conditions the same (Li *et al.* 1994). The larger deviations from the heavy+heavy–light kinematic limit (given by $P_2=-0{\cdot}5$) as the size of the radical group increases is noticeable.

Not only can the deviation from the kinematic limit lead to a lack of strong polarization of the product rotational angular momentum. It may also be due to the presence of the product orbital angular momentum because of dynamical factors (see §4.4).

3.2. *MPI, CARS and other techniques*

In the case of LIF, one uses a tunable laser to induce absorption by the sample and to monitor its subsequent fluorescence. Instead, in MPI and CARS, a second laser, at fixed frequency, is used to ionize the sample once excited or to create a coherent emission of light (Hefter and Bergmann 1988, Demtröder 1992).

In the case of MPI, the photo-ions are extracted from the interaction volume by an external field, accelerated and collected with high efficiency. In this technique one, two, three etc. photons can be used as well to ionize the sample ((1+1), (1+2), (1+3) ...processes); the response of the system is enhanced when the photon frequency coincides or is close to an energy difference between intermediate molecular levels (REMPI) (Meier *et al.* 1985, Jacobs *et al.* 1986). The stationary population density is obtained by solving usual rate equations using absorption, emission and ionization cross-sections. Their solution shows that the intensity of the second laser has to be much larger than that of the first (tunable) laser, which means that, in practice, high intensity and high repetition rate pulsed lasers must be used. As a consequence of the resulting saturation, the absolute population calibration versus laser intensity is an even more complicated problem than for LIF; it can only be solved in the case of a resonant (1+1) process (Jacobs and Zare 1986). Due to the large spectral width of pulsed lasers, profile analysis is generally not possible for chemical reactions at

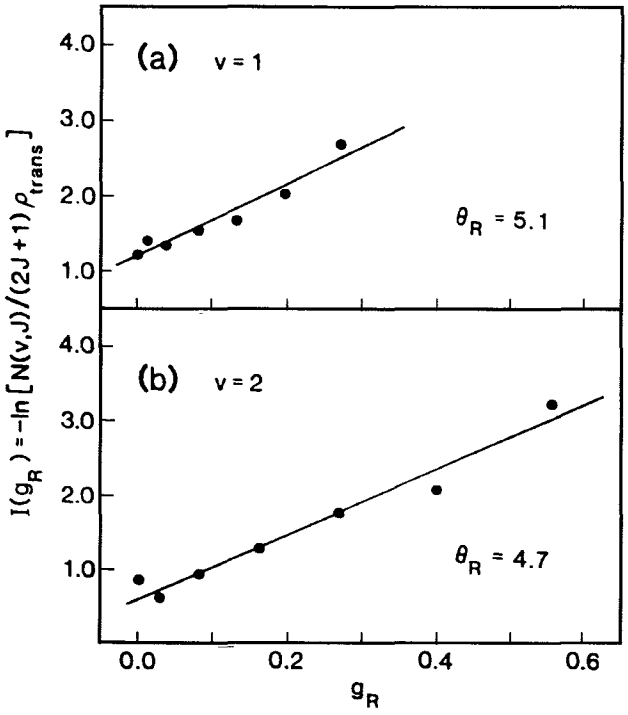

Figure 10. HD rotational distribution obtained for $v = 1$ and 2 from the reaction $H + D_2 \rightarrow HD + D$ using REMPI technique (adapted from Marinero *et al.* (1984)).

thermal energy. On the contrary, as the technique is very sensitive, it was used in the particular case of the $H + D_2 \rightarrow HD + D$ exchange reaction—with very small cross-section—to determine the rotational distributions at various collision energies by Zare and co-workers (Marinero *et al.* 1984). The state-specific detection of HD products could be accomplished by resonant two-photon UV excitation to the double minimum E, F $^1\Sigma_s^+$ state. Once this state is reached, a subsequent photon is absorbed to produce the HD^+ ion which is collected. In addition, mass spectroscopy is used to separate the desired ions from the ones created. In addition, mass spectroscopy is used to separate the desired ions from the ones created by the intense UV laser source. The HD rotational distributions obtained for $v = 1, 2$ are shown in figure 10.

The reactions of $O(^1D)$ atoms with HCl, OCl and Cl_2 molecules were studied by the same (2 + 1) REMPI technique (Shatter and Bershom 1991). The first reaction, which leads either to OH + Cl or to OCl + H products, has shown a large isotopic effect since the yields with HCl reagents are always larger than those of the DCl reagents. From this result, it could be concluded that the two products are formed via different mechanisms: abstraction in the first case, insertion in the second. Actually, the reaction which leads to OH + Cl products offers two reaction paths

$$\begin{array}{l} \qquad\qquad\qquad\quad OD(^2\Pi) + Cl(^2P_{1/2}) \\ \qquad\qquad\qquad\quad \nearrow \\ O(^1D) + DCl \\ \qquad\qquad\qquad\quad \searrow \\ \qquad\qquad\qquad\quad OD(^2\Pi) + Cl(^2P_{3/2}) \end{array}$$

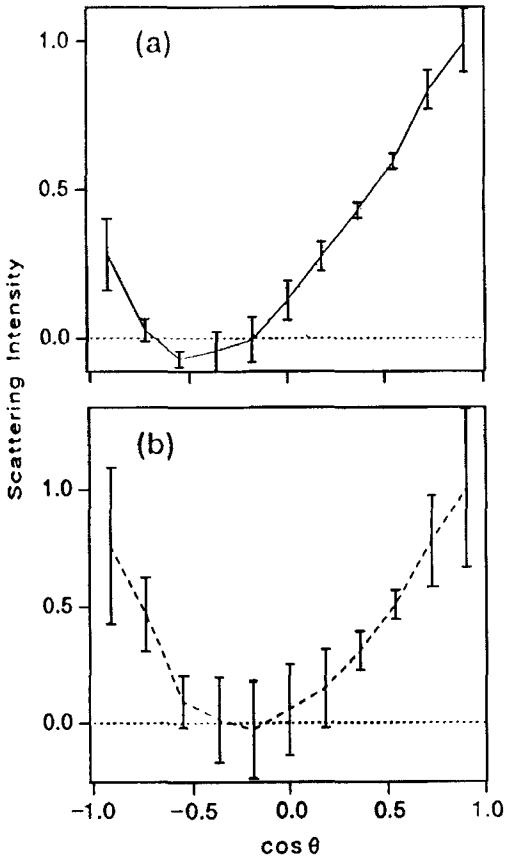

Figure 11. Extracted differential cross-section for (*a*) HCl($v' = 1, J' = 1$) and (*b*) HCl($v' = 1, J' = 3$) from the reaction $Cl(^3P_{3/2}) + CH_4(v_3 = 1, J = 1)$ at centre-of-mass collision energy 0·159 eV (adapted from Simpson *et al.* (1993)).

From the measurement of the branching ratio $[Cl(^2P_{1/2})]/[Cl(^2P_{3/2})]$, it could be concluded that the two reaction paths are non-adiabatic.

Production of hot reagent atoms in a bulk (§2) and application of the LIF or REMPI techniques of detection can be used for the measurement of product angular distributions in state-to-state reactions (Shatter *et al.* 1993). Although there are some limitations inherent to this new technique, it clearly represents a step forward in the study of reaction dynamics, which is complementary to high-resolution cross-beam experiments. It may gain a significant enhancement in signal-to-noise ratio, but it is restricted to reactions with favourable energetics and mass combinations.

Figure 11 shows the HCl differential cross-sections resulting from the $Cl(^3P_{3/2}) + CH_4$ ($v_3 = 1, J = 1$) reaction, for two rotational levels of HCl ($v = 1$) at a c.m. energy of 0·159 eV (Simpson *et al.* 1993). The reaction was initiated in a mixture of methane and chlorine in helium carrier gas by laser photolysis of Cl_2 at 355 nm, whereas methane molecules were excited into the ($v_3 = 1, J = 1$) asymmetric stretch mode by infrared absorption. Following a 100 ns time delay to allow for reaction, the HCl products could be probed by a (2 + 1) resonance-enhanced multiphoton ionization which led to the determination of the differential cross-sections for two specific rotational levels of $v' = 1$. The data analysis demonstrated interesting dynamics

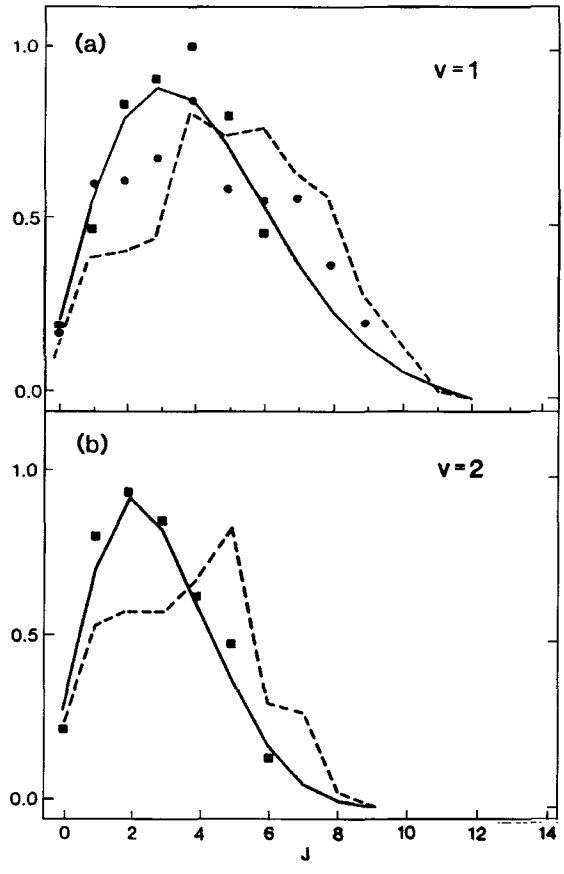

Figure 12. Rotational distribution of the nascent HD formed from the $H+D_2 \rightarrow HD+D$ reaction. Filled points are experimental results obtained by REMPI (adapted from Marinero *et al.* (1984)) (filled squares) and CARS from Gerity *et al.* (1983) (filled circles). Full curve is a theoretical fit from surprised analysis, dashed curve is the theoretical results from quasi-classical trajectory calculations (adapted from Blais and Trublar (1983)).

leading to forward scattering rotationally cold HCl products, consistent with an impulsive interaction along a quasi-linear Cl–H–CH_3 transition state.

In CARS (Druet and Taran 1981), two laser beams at frequency ω_1 and ω_2 are focused in the reaction volume. When the frequency difference $\omega_a = \omega_1 - \omega_2$ is equal to a Raman frequency of the molecular product, a nonlinear polarization of the medium is induced for collinear beams, resulting from the 'phase-matching' condition about wave vectors: $\mathbf{k}_a = 2\mathbf{k}_1 - \mathbf{k}_2$. Then, an anti-Stokes wave travels along the common direction of the two beams at the frequency ω_a. Its intensity is proportional to the population density of the initial level and to the product of the laser intensities. The advantage of the technique is that it can be applied to molecules without permanent dipole, such as H_2 or N_2 which do not absorb in the visible spectrum. This is precisely why it could be applied by Valentini and co-workers (Nieh and Valentini 1988, 1990) to characterize the $H + D_2 \rightarrow HD + D$ reaction. For illustration, rotational distributions are shown in figure 12 for $v = 1$ and 2, together with results of quasi-classical trajectory calculations (Blais and Trublar 1983).

The high sensitivity of the CARS technique has been applied to the investigation of quenching and photochemical processes in collisions between Na(3p) excited atoms and hydrogen molecules in a series of bulk experiments (Pichler *et al.* 1992, Motkus *et al.* 1992). This system, which was studied theoretically in great detail, offers interesting properties as it leads to the formation of NaH molecules and crystallites, although the initial $Na(3p)+H_2 \rightarrow NaH+H$ photochemical reaction is endoergic by 0·5 e. Owing to time-resolved experiments, it could be shown that NaH molecules are probably not formed via the two-step process involving energy-pooling collisions

$$Na(3p)+Na(3p) \rightarrow Na(5s, 4d)+Na(3s)$$

$$Na(5s, 4d)+H_2 \rightarrow NaH+H$$

but rather via the following quenching mechanism leading to vibrationally hot hydrogen molecules

$$Na(3p)+H_2(v''=0) \rightarrow Na(3s)+H_2(v''=1,2,3)$$

$$Na(3p)+H_2(v''=1,2,3) \rightarrow NaH+H$$

The NaH loss which occurs later was attributed to cluster formation, as is probably the case in caesium and hydrogen mixtures ('laser snow', Tam *et al.* (1975)). In further developments, degenerate four-wave mixing spectroscopy was used to determine rotational and vibrational temperatures in the NaH formation following the previous reaction (Motzkus *et al.* 1992).

3.2.1. *Reaction product imaging*

Recently a new technique for obtaining differential cross-sections with both product state resolution and simultaneous detection of all scattering angles has been developed. It is called reaction product imaging (Suits *et al.* 1992, Kitsopoulos *et al.* 1993). In this technique the three-dimensional velocity distribution of state-selected reaction products is determined by ionizing the desired reaction product, and subsequently accelerating the ion onto a position sensitive detector. The ion images appearing on the detector are two-dimensional projections of the three-dimensional product velocity distribution. Whereas visual inspection provides immediate qualitative information about the reaction, mathematical analysis can provide detailed differential cross-sections. Ion imaging techniques began in 1987 (Chandler and Houston 1987) for the measurement of photofragment velocity distributions (speed and angle) from unimolecular dissociation processes. One of the interesting features of the technique relies on the fact that only one image is all that is required to define uniquely the three-dimensional (3D) angular distribution. This novel technique has been used to investigate the inelastic collision process

$$Ar+NO(^2\Pi_{1/2}, v=0, J=0,5) \rightarrow Ar+NO(^2\Pi_{1/2}, v=0, J')$$

at collision energy of 0·21 eV by Suits *et al.* (1992). This ion imaging technique has also been applied for the measurement of the differential cross-section for the $H+D_2 \rightarrow HD+D$ reaction in which the D atom product was imaged (Kitsopoulos *et al.* 1993). The reaction was studied at relative collision energies of 0·54 and 1·29 eV. By integration of the intensity of the reconstructed images, the experimental angular

distribution can be estimated allowing for quantitative comparison with theoretical calculations. The obtained differential cross-section for D atom production showed forward scattering in overall good agreement with quasi-classical trajectory calculations, carried out by Aoiz *et al.* 1992, based on the LSTH (Liu–Siegebahm–Truhlar–Horowitz) potential energy surface.

4. Characterization of reaction products by chemiluminescence

When the chemical reaction is highly exoergic, a significant fraction of the products can be formed in electronically excited states. This feature was recognized in bulk experiments in early reaction dynamics studies (Polanyi 1932) and was observed later in molecular beam experiments (Jonah *et al.* 1972). Typically, the product internal distributions for atom exchange reactions are determined by measuring their vibrationally and rotationally-resolved infrared chemiluminescence spectrum under single-collision conditions, by the use of fast time-resolved Fourier transform spectroscopy (Aker and Sloan 1985). In the following, reference is made to ultraviolet or visible chemiluminescence. After proper detection and spectral analysis, chemiluminescence spectra can be used for the determination of reaction dynamics and stereodynamics, essentially from the measurement of total and partial cross-sections and from the analysis of polarization data.

4.1. *Total cross-section measurements*

For chemiluminescent reactions involving electronically excited reagents, a novel method of determining absolute densities of particles has been developed (Dagdigian 1978). Let us consider the $M^* + XY \rightarrow MX^* + Y$ reaction. The intensity of the signal related to the fluorescence emission of a metastable atom is connected with its emission rate R_M^* by

$$I_M^* = R_M^* \Delta V \delta\eta \left(\frac{\Omega}{4\pi}\right) = n_M^* \Delta V \delta\eta \left(\frac{\Omega}{4\pi} \tau_M^*\right) \tag{31}$$

in which, as before, ΔV is the emission volume, $\delta\eta$ is the overall collection and detection efficiency, and Ω is the solid angle of collection. Here, R_M^* is equal to the number density n_M^* divided by the lifetime τ_M^* of the excited atom since, on average, one photon is emitted in each period τ_M^* if one excited atom permanently exists in the emission volume. In the same manner, the chemiluminescent emission of the MX* products is related to their emission rate R_{MX}^* by

$$I_{MX}^* = R_{MX}^* \Delta V \delta\eta \left(\frac{\Omega}{4\pi}\right). \tag{32}$$

By analogy with equation (1), the chemiluminescence cross-section is defined as

$$\sigma_{\text{chemi}} = \left(\frac{dN_{MX^*}}{dt}\right)(n_M^* n_{XY} v_r \Delta V)^{-1} = \left(\frac{I_{MX}^*}{I_M^*}\right)(n_{XY} v_r \tau_M^*)^{-1}. \tag{33}$$

The major purpose of the method is that the measurement *in situ* of the light emission due to the metastable atom and the reaction products eliminates, upon normalization, all the difficulties associated with the calibration of the excited reagent density, the size of the emission volume, the solid angle of collection and the detection efficiency.

Figure 13 displays the chemiluminescence spectrum for the $Ca(^1D_2) + HBr \rightarrow CaBr^* + H$ reaction (Garay *et al.* 1995). The spectral range selected includes both A–X

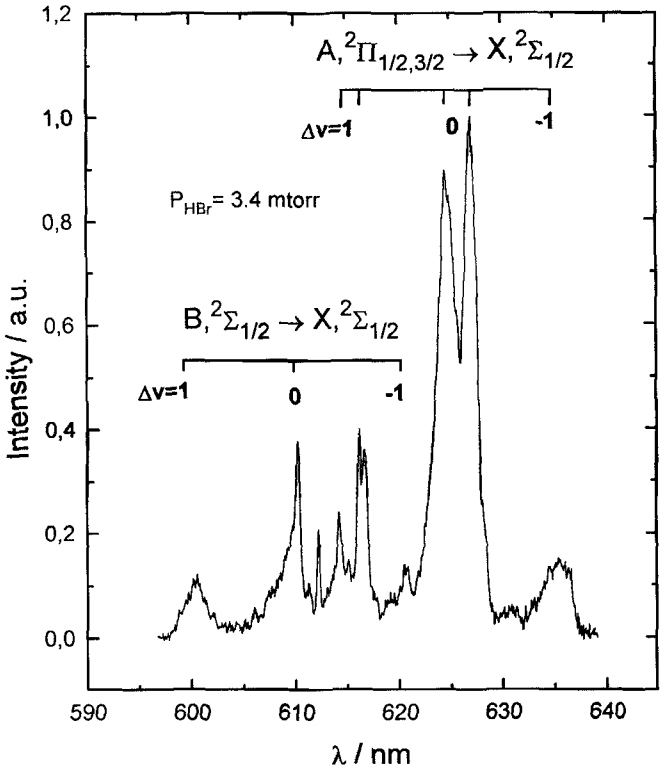

Figure 13. Chemiluminescence spectrum for the $Ca(^1D_2) + HBr \rightarrow CaBr^* + {}^*H$ reaction. Both A and B–X molecular bands with their $\Delta v = 0 \pm 1$ sequences are depicted.

Table 2. Absolute values of σ_R obtained for several chemiluminescent reactions.

Reaction	$\sigma_R(Å^2)$	Ref.
$Ca(^3P) + SF_6 \rightarrow CaF(A) + SF_5$	0·54	Verdasco *et al.* (1987)
$Ca(^3P) + SF_6 \rightarrow CaF(B) + SF_5$	0·12	Verdasco *et al.* (1987)
$Ca(^1D) + SF_6 \rightarrow CaF(A) + SF_5$	0·59	Verdasco *et al.* (1987)
$Ca(^1D) + SF_6 \rightarrow CaF(B) + SF_5$	0·04	Verdasco *et al.* (1987)
$Ca(^3P) + Cl_4C \rightarrow CaCl + Cl_3C$	0·25	Verdasco *et al.* (1990)
$Ca(^1D) + Cl_4C \rightarrow CaCl + Cl_3C$	1·77	Verdasco *et al.* (1990)
$Ca(^3P) + N_2O \rightarrow CaO + N_2$	4·80	Irvin and Dagdigian (1981)
$Ca(^1D) + N_2O \rightarrow CaO + N_2$	3·60	Irvin and Dagdigian (1981)
$Ca(^1D_2) + HCl \rightarrow CaCl(A) + H$	1·04 ± 0·17	Menéndez *et al.* (1993)
$Ca(^1D_2) + HCl \rightarrow CaCl(B) + H$	0·14 ± 0·02	Menéndez *et al.* (1993)
$Ca(^1D_2) + HCl \rightarrow CaBr(A) + H$	2·2 ± 0·9	Menéndez *et al.* (1993)
$Ca(^1D_2) + HBr \rightarrow CaBr(B) + H$	0·52 ± 0·24	Garay *et al.* (1995)
$Ca(^1D_2) + CH_3OH \rightarrow CaOH(A) + CH_3$	0·011 ± 0·005	Esteban *et al.* (1994)
$Ca(^1D_2) + C_2H_5OH \rightarrow CaOH(A) + C_2H_5$	0·007 ± 0·004	Esteban *et al.* (1994)
$Ca(^1D_2) + CH_3OH \rightarrow CaOH(B) + CH_3$	0·003 ± 0·001	Esteban *et al.* (1994)
$Ca(^1D_2) + C_2H_5OH \rightarrow CaOH(B) + C_2H_5$	0·001 ± 0·0006	Esteban *et al.* (1994)
$Ca(^3P_J) + CH_3OH \rightarrow CaOH(A) + CH_3$	0·002 ± 0·001	Esteban *et al.* (1994)
$Ca(^3P_J) + CH_3OH + CaOH(B) + CH_3$	0·0004 ± 0·002	Esteban *et al.* (1994)

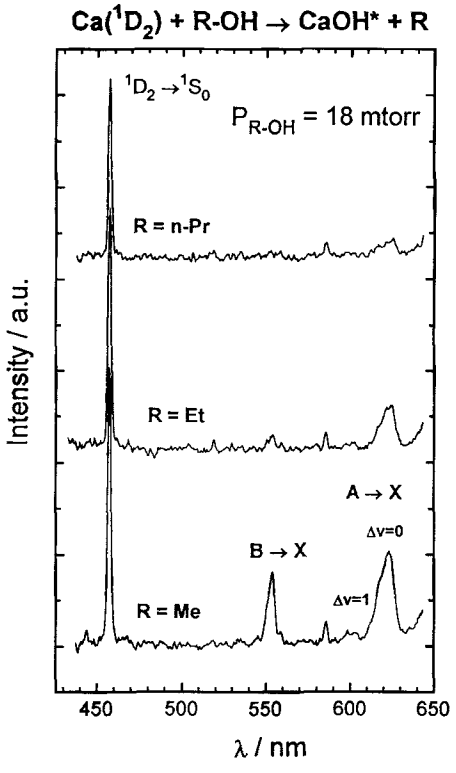

Figure 14. Chemiluminescence spectra (corrected with the spectral response) for the Ca* + ROH reactions: (upper trace) propanol, (middle) ethanol and (lower) methanol (adapted from Esteban *et al.* (1994)).

and B–X molecular emission bands of CaBr, with their $\Delta v = 0, \pm 1$ sequences. Figure 14 displays the three chemiluminescence spectra corresponding to the Ca* + ROH → CaOH + R reaction family, with R = CH_3, C_2H_5 and C_3H_7. The spectra show similar overall features, e.g. the Ca($^1D_2 \rightarrow {}^1S_0$) metastable emission and two broad molecular bands centred at 554 and 623 nm. From the integrated intensities and a proper calibration of the signal versus the spectral response of the set-up, one obtains absolute chemiluminescent cross-sections (table 2), in which it is interesting to note the negative dependence of the Ca* + ROH cross-sections as the radical group increases, a trend explained by more steric hindrance versus the size of the group.

In a different technique, the Ca(^3P_j) + $CH_3I \rightarrow$ CaI (A, B) + CH_3 chemiluminescent reaction is induced by laser excitation of calcium atoms in the presence of CH_3I and helium buffer gas at high temperature (Basterrechea *et al.* 1991). Figure 15 displays the corresponding broad band spectrum (spectral resolution ≈ 4 nm) with the Ca($4s4p\,^3P_j \rightarrow 4s^2\,^1S_0$) resonance emission at 657 nm and the combined CaI($A\,^2\Pi$, $B\,^2\Sigma^+ \rightarrow X\,^2\Sigma^+$) systems where the sequences $\Delta v = 0, \pm 1$ are separated.

4.2. *Product internal state distributions*

Due to the high degree of product internal excitation and to the typically low spectral resolution, chemiluminescent spectra are not well-resolved, so a decon-

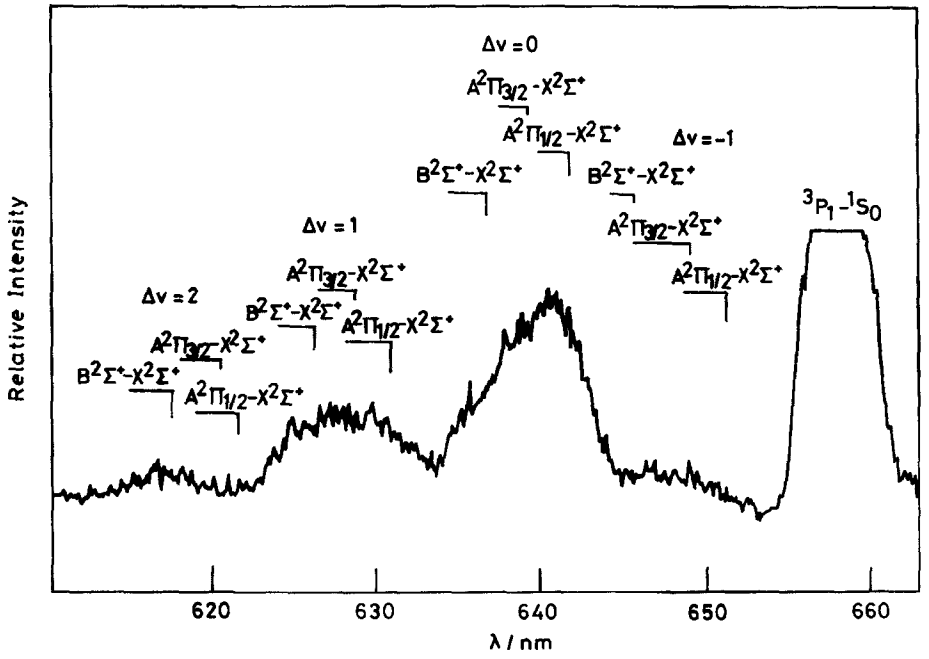

Figure 15. Example of the laser-induced chemiluminescence technique for the $Ca(^3P_1) + CH_3I \rightarrow CaI(A, B) + CH_3$ reaction. It is shown a broad band chemiluminescence spectrum (optical resolution ~ 4 nm) indicating atomic resonance fluorescence emission at $\lambda = 657{\cdot}3$ nm $Ca(4s4p(^3P_1) \rightarrow Ca\ (4s^2(^1S_0))$ and molecular chemiluminescent emission from the combined $CaI(A^2\Pi, B^2\Sigma^+ \rightarrow X^2\Sigma^+)$ systems ($\Delta v = 0$, 1 and 2 sequences) following the pulsed dye-laser generation of $Ca(^3P_1)$ from atomic calcium vapour in the presence of CH_3I and helium buffer gas at elevated temperature (adapted from Basterrechea *et al.* (1991)).

volution is often required to extract the corresponding distributions. Although regression techniques have been used (Johnson *et al.* 1983, Prisant and Zare 1985), the usual procedure consists of varying the product state population in an iterative manner until the simulated spectrum reproduces the experimental one, functional forms being used for both vibrational and rotational distributions to avoid too much scatter in the calculated populations. Figure 16 shows the vibrational distribution of the CuF(B) state following the $Cu(^2S) + F_2 \rightarrow CuF + F$ reaction, where the average fraction of energy for product vibration is higher than for a 'prior' distribution (Levine and Bernstein 1987) and, consequently, very little is left for translational excitation (Parson and Fang 1990).

4.3. *Product angular distributions*

When chemiluminescent products have a long radiative lifetime, they are able to travel a significant distance before radiation takes place. This feature can be used to measure the angular distribution of the nascent products (Mims and Brophy 1977, Siegel and Schultz 1978) with additional information on their lifetime and identity. For the $Ba + N_2O$ reaction, the angular distribution suggested a significant yield of the long-lived BaO $A\,^2\Pi$ state, in addition to that of $A\,^1\Sigma^+$.

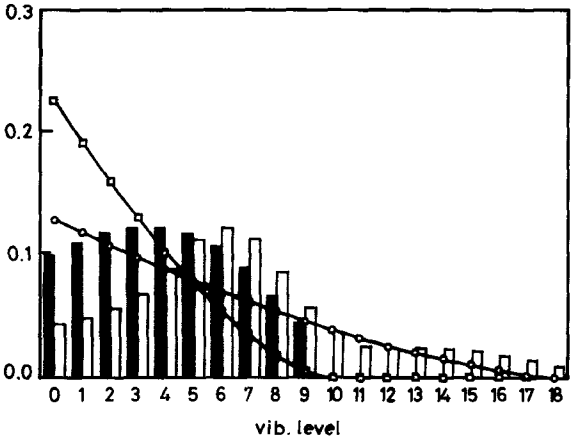

Figure 16. Vibrational distribution of CuF in the b state formed from $Cu(^2S)+F_2 \rightarrow CuF+F$ at collision energies of 11 kJ mol^{-1} (solid columns) and 67 kJ mol^{-1} (open columns). Corresponding prior predictions are squares and open circles (adapted from Parson and Fang (1990)).

4.4. *Product polarization and stereodynamics*

Information about the stereodynamics can also be obtained by measuring polarized chemiluminescence spectra. Figure 17 shows an example of a pair of perpendicular and parallel polarized spectra for the CaBr* produced in the $Ca(^1D)+HBr \rightarrow CaBr(A,B)+H$ reaction. As can been seen, both the A–X and the parallel B–X transition intensities are very sensitive to the polarization direction, as was expected for this kinematically-constrained reaction.

For a selected molecular transition, the polarization degree, defined by the expression

$$P = \frac{I_{\parallel} - I_{\perp}}{I_{\parallel} + I_{\perp}} \tag{34}$$

can be obtained from the direct integration of the measured spectra to have the parallel, $I_{\parallel}$ and perpendicular $I_{\perp}$, emission intensities. This magnitude has been calculated for the B–X molecular band, because the polarization analysis of a parallel transition gives the rotational alignment parameter of the molecule, $\langle P_2(\mathbf{j}'\cdot\mathbf{k})\rangle$, through simple relations (Prisant *et al.* 1981). In the following discussion, $\mathbf{j}'$, $\mathbf{k}$ and $\mathbf{z}$ represent the unitary vectors of the rotational product angular momentum, relative velocity and atomic beam velocity. As is known for these transitions, P and the value of $\langle P_2(\mathbf{j}'\cdot\mathbf{z})\rangle$ are related by the expression (Prisant *et al.* 1981)

$$P = \frac{3\langle P_2(\mathbf{j}'\cdot\mathbf{z})\rangle}{\langle P_2(\mathbf{j}'\cdot\mathbf{z})\rangle - 4}. \tag{35}$$

The azimuthal average addition (AAA) theorem (Johnson *et al.* 1984) is used to correct the beam-gas blurring effect of the rotational alignment given by $\langle P_2(\mathbf{j}'\cdot\mathbf{z})\rangle$, e.g.

$$\langle P_2(\mathbf{j}'\cdot\mathbf{z})\rangle = \langle P_2(\mathbf{j}'\cdot\mathbf{k})\rangle\langle P_2(\mathbf{k}'\cdot\mathbf{z})\rangle. \tag{36}$$

To obtain $\langle P_2(\mathbf{k}\cdot\mathbf{z})\rangle$ one follows the procedure described in Prisant *et al.* (1981), whose details are omitted for brevity. This allows us to calculate the rotational

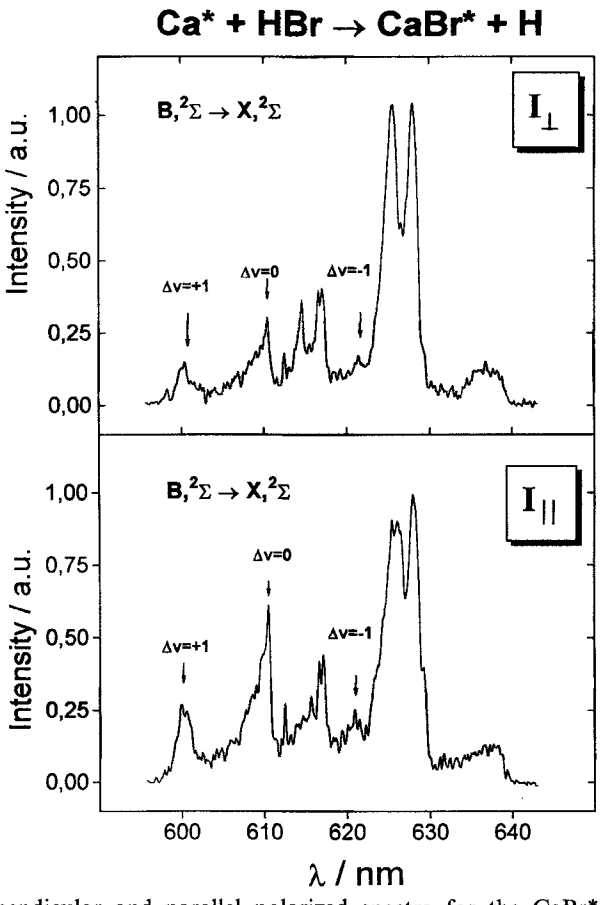

Figure 17. Perpendicular and parallel polarized spectra for the CaBr* produced in the $Ca(^1D_2)+HBr \rightarrow CaBr(A_1, B)+H$ reaction. Note the sensitivity to the polarization direction as can be expected for this kinematically-constrained reaction (adapted from Garay *et al.* (1995)).

alignment referred to as the centre-of-mass system. Table 1 contains the alignment parameters for a series of reactions. Note the closeness to the kinematic limit, given by $\langle P_2 \rangle = -0{\cdot}5$, as the system approaches the heavy plus heavy–light limit (§2.2).

Significant deviations from the kinematic limit given by the perfect alignment of the product rotational angular momentum have been reported, particularly at low collision energies. Obviously, such deviations indicate the occurrence of disposal of angular momentum into product orbital motion. As an example of a dynamical model that accounts for these deviations from perfect alignment one can mention the so-called constant product orbital angular momentum (CPOAM) (Hartree *et al.* 1990). One of the basic assumptions of the CPOAM model is the recognition of a constant-product orbital angular momentum, L', when the departing atom is very light in comparison with its diatomic partner. One of the main results of such an approach is given by the following expression for the alignment parameter (Hartree *et al.* 1990)

$$\langle P_2(\mathbf{J}' \cdot \mathbf{k}) \rangle = Z^2 m(\tfrac{1}{3} - \ln Zm) - \tfrac{1}{2} \tag{37}$$

where $Zm = L'/L_m$, and L_m is the maximum angular orbital momentum proportional to the average energy available.

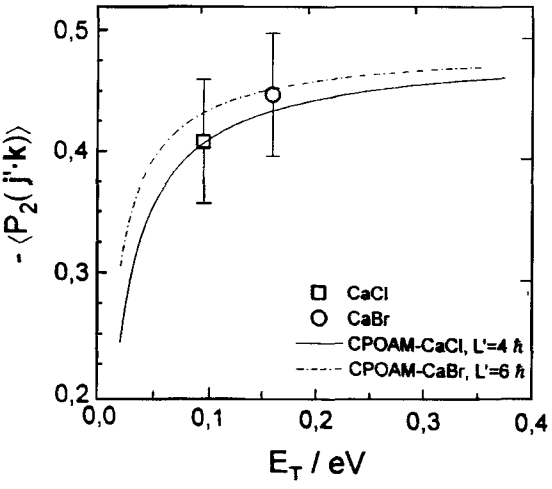

Figure 18. Experimental versus theoretical values of the product rotational alignment for the $Ca^* + HX(X = Cl, Br) \rightarrow CaX^* + H$ reaction. Calculated values are model predictions using the COPAM model (see text) (adapted from Garay *et al.* (1995)).

Figure 18 compares the experimental and theoretical values of the product rotational alignment for the $Ca^* + HX(X = Cl, Br) \rightarrow CaX^* + H$ reactions. The closeness to the kinematic limit and the capability of the CPOAM model should be noted.

In general, whereas there are many examples of the $\mathbf{L} \rightarrow \mathbf{j}'$ correlation little is known about the second correlation, i.e. the complete transfer of $\mathbf{j}$ into $\mathbf{L}'$. Recently extensive quasi-classical trajectory calculations have been carried out to study such correlations in the $Ba + HI \rightarrow BaI + H$ system (Alberti *et al.* 1995). In this work the variation of $\langle \mathbf{L}' \rangle$ with $\mathbf{j}$ was found to show a linear dependence. The later vector correlation leads to two important consequences. The first deals with the scalar description. As reported, the higher the rotational excitation of the reagents the higher the product orbital angular momentum. The second aspect of this well reached kinematic limit deals with the vectorial character of the magnitude to be transferred. As $\mathbf{j} \rightarrow \mathbf{L}'$ and $\mathbf{L}$ is always perpendicular to $\mathbf{v}'$, the product velocity, one could select the product velocity vector to the desired laboratory direction by selecting the reagent rotational angular momentum polarization. Of course, this is equivalent to selecting the collision plane, which in turn opens up interesting possibilities concerning the spatial control of the reaction product. In fact, the spatial control of the reaction product by laser polarization is quite obvious in photofragmentation dynamics of both diatomic and linear polyatomic molecules (Schinke 1993). What is now being emphasized is the extension of such a possibility for atom exchange reactions for kinematically-constrained reactions.

As far as the reactivity of oriented molecules is concerned, an interesting study was recently carried out by Ohoyama *et al.* (1993) who measured the chemiluminescence emission of CF_3^* produced in the reaction of $Ar(^3P)$ with oriented CF_3H molecules. As has been well-known since the 1960s, the usual method of orienting molecules in a beam has been the electrostatic hexapole technique (Stolte 1988). This study follows the well-known BaO* chemiluminescence yield from the crossed-beam reaction of N_2O plus Ba atoms (Stolte 1988) based on the hexapole technique to orient and state select the N_2O molecules.

Recently, the possibility of orienting molecules in the gas phase by means of homogeneous strong electric fields, the so-called brute force orientation technique, has been demonstrated by Loesch and Reincheild (1990) and a little later, independently, by Friedrich and Herschbach (1991). Although this technique finds wider application than the conventional hexapole method, to the best of the authors' knowledge no experimental work has been reported using this method, in a crossed-beam experiment, with either chemiluminescence or laser detection techniques.

5. Dynamics of excited-state reagents

Long before the development of laser techniques, classical techniques—electron bombardment, electronic discharges (Pauly 1988)—were used to prepare atomic/molecular reagents in chemical reactions. They present the disadvantage of being highly non-selective in energy so that a number of atomic/molecular states of largely different energy are simultaneously populated. In turn, this situation can be considered as favourable to populate metastable levels with a low optically-allowed transition probability from the ground state. A certain selectivity is recovered when the excitation is performed far from the collision volume, since only metastables have a long enough lifetime to survive and proceed to reaction.

Optical techniques with tunable lasers are more flexible, versatile and efficient (Bergmann 1988). This is because the interfacing of particle beams and laser beams can be realized directly at the collision volume; hence the possibility of exciting short-lived atomic/molecular states, just by tuning the laser frequency. In the case in which direct electronic transitions are not allowed, two-photon or two-step processes can remedy the situation. However, the main interest of electronic excitation by lasers lies in its selective character: up to the fine/hyperfine structure of the atom (Jacquinot 1976) or up to the vibrational/rotational structure of the molecular reagent (Bergmann 1988). Moreover, due to the Doppler effect, this excitation can be carried out for a given class of velocity which depends on the beam geometrical arrangement and on the laser frequency. For a perpendicular arrangement, all the classes of velocity should absorb the laser radiation leading to an important transfer of population. Also, it is possible to use the polarized and coherent nature of the laser field to observe other phenomena: influence of polarization on the reactivity, 'driving' of chemical reactions by intense laser fields.

However, the situation described above presents some drawbacks. In practice, the population of excited states can be very low, in particular for atomic reagents: in principle, the amount of transferred population from the ground state is proportional to the transition probability and to the spectral energy density, but due to saturation effects and to 'side-transitions', it is far from the 50% limit which could be obtained in pure two-level systems (Walther 1976, Shimoda 1976, Demtröder 1982). Conversely, for molecular reagents, the STIRAP technique, which has been developed recently, is very efficient in populating a given specific rovibrational level—but at the cost of a complex experimental arrangement (Gaubatz *et al.* 1989, Schiemann *et al.* 1993). There are also specific drawbacks linked to reaction dynamics. For instance, as the degree of reagent excitation becomes higher, more excited states are populated (just by spontaneous emission) and are able to contribute to the reaction: as a consequence, the signal is lower and the selective character of the excitation is lost.

Whereas in §§3 and 4 the emphasis was put on product detection and characterization as a route to obtain information about the reaction dynamics, the

present section is devoted to the study of the influence of selective reagent excitation by optical methods. The reader is addressed to Stolte (1988) and Lee (1988) for a discussion on state-selected reagent excitation by non-optical methods. Nevertheless we start this section with a brief account of recent work on translational energy effects on the reaction cross-section.

5.1. *Collision energy effects*

For neutral–neutral interactions, as far as the collision energy dependence of the reaction cross-section is concerned, three methods have frequently been used in order to vary the relative translational energy of the reagents. They involve the variation of:

(i) the velocity of one or both of the beams;
(ii) the collision angle; and
(iii) the time of flight of at least one reagent.

In the former, the typical implementation consists of changing the relative velocity by varying one beam velocity via the seeding technique. Many applications of this method have been reported and the reader is addressed to a review article (González Ureña 1987) for further information. The changing of the collision geometry, i.e. the change of the collision angle, while both beam velocities remain fixed, in spite of its simplicity, has only been applied in a very few cases for inelastic transitions, although reactive collision experiments using this method have only been reported by Verdasco *et al.* (1989). The philosophy of the time-of-flight (TOF) method is based on the collision of one stationary target (either beam or gas) which collides with a pulsed beam. If reaction takes place, the measurement of the reagent time-of-flight spectrum as well as the product time profile gives the time and hence the collision energy dependent reaction cross-section via the modified equation

$$\sigma_R(E|t) = \frac{F_{AB}(t)}{n_A(t) n_{BC} V_R(t) \Delta V} \tag{38}$$

in which we have assumed BC as stationary. This method has been used for beam-gas experiments and, not as often, for crossed-beams (Wicke 1983).

In fact a nominal reactive rate coefficient as a function of the average collision energy can be calculated by dividing the chemiluminescence intensity $F_{AB}(t)$ by the reactant number density $n_A(t)$, e.g. rearranging equation (38) one obtains for the specific rate constant

$$k(E|t) = \sigma_R(E|t)\, V_R(t) = \frac{F_{AB}(t)}{n_{BC} \Delta V n_A(t)} \tag{39}$$

so that $k(E|t)$ is proportional to $F_{AB}(t)/n_A(t)$ since ΔV and n_{BC} are not time-of-flight dependent quantities.

Figure 19 shows several specific rate constant examples obtained with this time-of-flight method. One of the most significant aspects of the method is its high sensitivity in the measurement of the excitation function. In fact, the high sensitivity in the collision energy associated with an energy spread of a few millielectronvolts can unravel non-classical effects in the excitation functions. See for example Menéndez *et al.* (1993) for a discussion of this point.

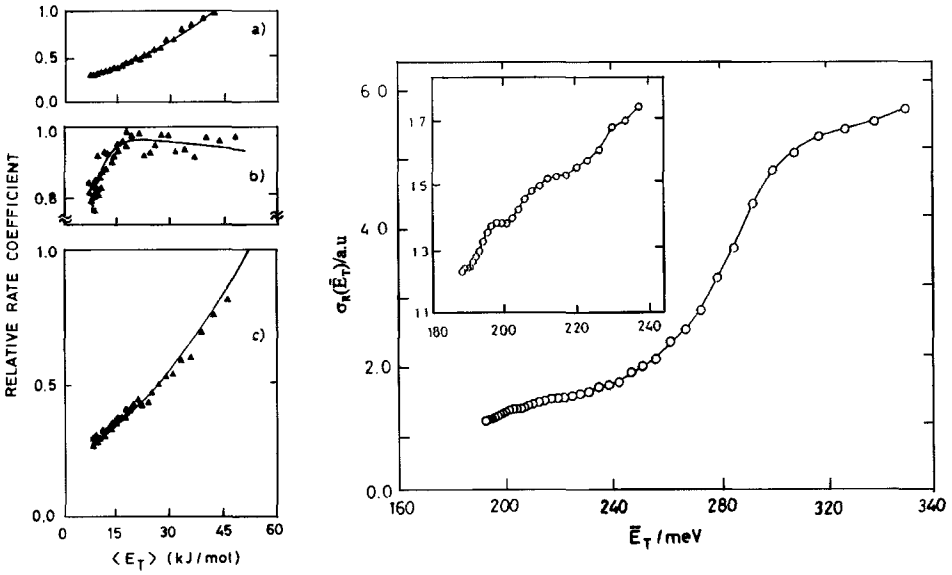

Figure 19. Comparison of several specific rate constants and reaction cross-sections obtained by the time profile measurement of cross-beam chemiluminescence. Left: (a) CuF ($b\,^3\Pi$) from Cu(^{2}S) + F_2; (b) CuF ($b\,^3\Pi$) from Cu(^{2}D) + F_2 and (c) CuF ($C^2\Pi$) from Cu(^{2}D) + F_2 (adapted from Parson and Fang (1990)); right: CaCl* from Ca($^1D_2$) + HCl reaction (adapted from Menéndez *et al.* (1993)).

5.2. *Electronic excitation: state-selected and spin–orbit effects*

In addition to the promotion of endoergic reactions which is permitted by the compensation of energy defects, electronic excitation is a most convenient means of studying state-selected and spin–orbit effects, a domain where new results are rapidly emerging. Spin–orbit effects in alkaline earths, halogens and inert gases were detailed less than a decade ago in a review article (Dagdigian and Campbell 1987), with a careful analysis of various adiabatic and non-adiabatic processes giving rise to specific variations of rate coefficients and cross-sections. Several aspects of electronic excitation which were not treated in the frame of that article or which appeared later are described in a recent review article (González Ureña and Vetter 1995) by considering their influence over total and differential cross-sections as well as over the state of reaction products. Thus, only a few examples will be discussed below.

A number of crossed-beam experiments by Lee and co-workers were devoted to the reactivity of excited sodium atoms (Vernon *et al.* 1986, Weiss *et al.* 1986, Mestdagh *et al.* 1987) and showed contrasting results. For instance, the NaCl total and differential cross-sections observed for the Na(3s ^{2}S, 3p ^{2}P) + $Cl_2 \rightarrow$ NaCl + Cl reactions do not exhibit large variations, although electronic excitation to the Na(3p) state lowers the atom ionization potential by 2·1 eV. On the contrary, as is shown in figure 20, the NaCl total and differential cross-sections observed for the Na(3s ^{2}S, 3p ^{2}P, 5s ^{2}S, 4d ^{2}D) + HCl $\rightarrow$ NaCl + H reactions are significantly different from Na(3s) to Na(4d). For the Na + O_2 system, excitation to Na(4d) leads to NaO products whereas excitation to Na(3p) and Na(5s) does not.

These reactions generally proceed via the harpooning mechanism which provides a good framework to explain the effect (or the non-effect) of electronic excitation over reactivity. For instance, the small enhancement of the cross-section from Na(3s) to Na(3p) for the reactions of Na with Cl_2 is surprising. One would expect that the atom

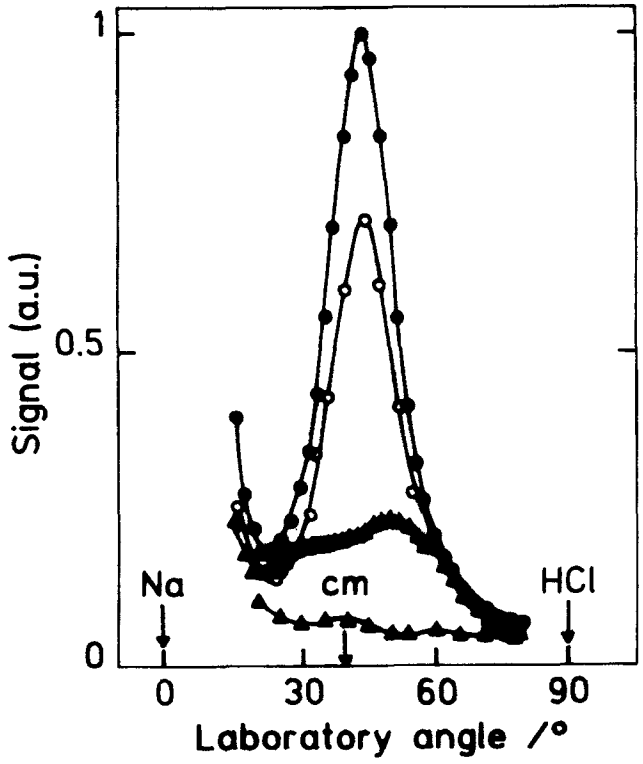

Figure 20. NaCl angular distribution for the Na + HCl → NaCl + H reaction at 56 kcal mol^{-1}, —▲— Na(3S) excitation (no reaction). ▲, Na(3P) excitation: ○, Na(5s) excitation: ●, Na(4s) excitation (adapted from Vernon *et al.* (1986)).

electronic excitation would increase the cross-section, just because the ionization potential is lowered; however, as the crossing distance between the covalent and the ionic potentials increases from Na(3s) to Na(3p), the interaction is reduced, making sodium atoms less reactive than they would otherwise be. It was finally argued that these two factors compensate each other to some extent. As for the reaction with hydrogen halides, the two dominant features of the reaction with excited atoms are the decreasing product recoil velocity and the increasing cross-section. For ground state reactions, the electron transfer does not take place at large distances because hydrogen halides have negative electron affinities; for the others, excited Na atoms have much lower ionization potentials and the electron transfer is possible at larger distances.

At a higher degree of selectivity, spin–orbit coupling is able to influence the atom reactivity, as was demonstrated by systematic measurements performed with calcium, strontium and barium atoms (Irvin and Dagdigian 1981, Yuh and Dagdigian 1983, Campbell and Dagdigian 1986, Dagdigian and Campbell 1987). For the reactions of Ca($4p\ ^3P_{0,1,2}$) with Cl_2, the following ordering for cross-sections is observed: $\sigma(J = 2) > \sigma(J = 1) > \sigma(J = 0)$ for the CaCl excited products, whereas the inverse is observed for the ground state products. This selectivity is kept by changing Ca into Sr or by changing chlorine into alkyl bromides or iodides. Comparable spin–orbit effects were also detected in reactions involving Ba($5d\ ^3D_{1,2,3}$) atoms and Cl_2, Br_2 or CCl_4 molecules, with the same ordering for cross-sections. These reactions generally proceed by charge transfers occurring at the crossing of the neutral entrance valley and the ionic intermediate, with a preferential C_{2v} geometry of approach due to a

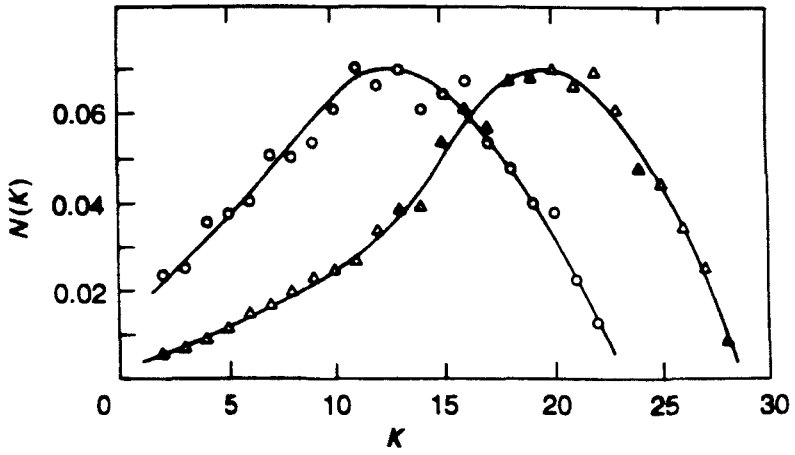

Figure 21. Initial rotational distribution of HgH products following $Hg(3P_1)$ and $Hg(3P_0)$ reactions with hydrogen molecules. △ $Hg(^3P_1)$ excitation. ○ $Hg(^3P_0)$ excitation (adapted from Bras *et al.* (1991)).

favourable overlap between reagent orbitals. As reactive cross-sections are very sensitive to the strength of neutral–ionic couplings, their ordering could be explained by using adiabatic correlation arguments.

Another consequence of spin–orbit dependence was demonstrated in a pump–probe study of the $Hg(6p\ ^3P_1, ^3P_0) + H_2 \rightarrow HgH(X\ ^2\Sigma) + H$ reactions and their isotopic derivatives (Bras 1990, Bras *et al.* 1991): as shown in figure 21, the absolute yield of HgH products is roughly the same for the two excitation schemes, but the rotational distribution corresponding to $Hg(^3P_0)$ is 'colder' than that of $Hg(^3P_1)$. This difference was explained invoking the existence of a substantial potential barrier on the adiabatic reaction path, higher for $Hg(^3P_0)$ than for $Hg(^3P_1)$.

In a series of crossed-beam studies performed on chemiluminescent reactions involving ($5d\ ^3D_2$, $5d\ ^1D_2$, $6p\ ^1P_1$) excited barium atoms and oxygen, water or alcohol molecules, it was shown how specific spin–orbit excitations can lead (or not) to specific products or product states, through well-defined reaction mechanisms (Mestdagh *et al.* 1990). For example, $Ba(6p\ ^1P_1)$ atoms reacting with water or alcohols do not lead to BaO products, but to $BaOH(A\ ^2\Pi)$ products rather than $BaOH(B\ ^2\Sigma^+)$ ones.

In principle two different mechanisms, described below, can be considered to account for the dynamics of the excited alkaline earth atom reaction with OH-containing molecules.

5.2.1. *Direct harpoon-type mechanism*

This involves a long-range interaction with electron transfer, i.e.

$$M^* + \begin{matrix} H \\ | \\ O\text{–}R \end{matrix} \rightarrow M^+ \ldots {}^-O \ldots R \rightarrow MOH^* + R$$

Because of its high electron affinity, the OH, isoelectronic with the F atom, acts as a whole entity accepting the electron from the attacking atom. As a result, there is no long-lived complex so that the R moiety departs as the attacking atom approaches. The whole process is so fast that there is no time for H migration or CaO formation. Essentially, this mechanism follows the well-known harpooning interaction between alkaline atoms with halogen-containing molecules.

5.2.2. *Long-lived intermediate via insertion mechanism*

Now the attacking atom inserts into the HOR molecule forming an adduct, i.e.

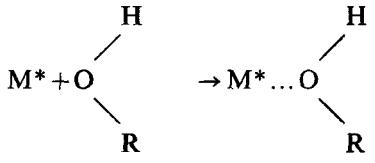

which, in turn, can evolve to different product channels as follows:

(a) O–H bond breaking with light atom recoil,

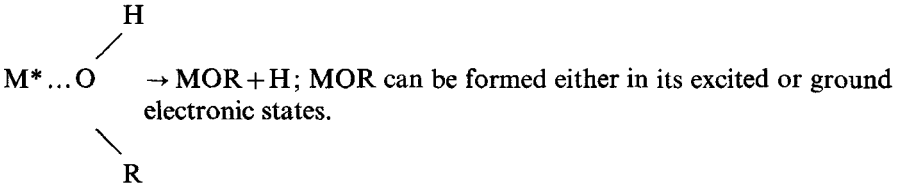

(b) O–R bond breaking with radical R recoil,

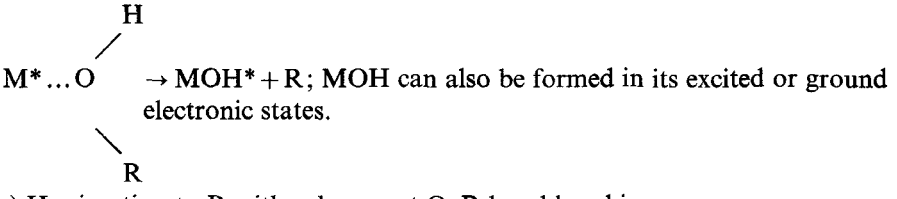

(c) H migration to R with subsequent O–R bond breaking, e.g.

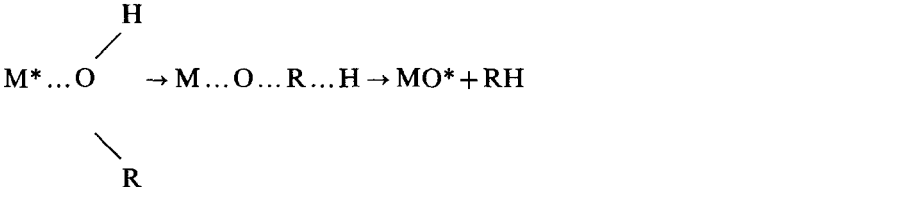

Whereas mechanism (a) has been suggested as the predominant one in the reaction of excited Ba with alcohols, in the excited calcium atom reactions $Ca^*(^1D_2) + ROH$ it appears that the CaOH* is the minor, but the only experimentally observed channel (Esteban *et al.* 1994). This is an indication that for energetically open channels not only the particular reaction pathway plays a role but also the stereodynamics associated with the reactive collision. There are good examples in the literature of such effects in addition to the already mentioned $Ca^*(^1D_2)$ attack to the RI molecule (Esteban *et al.* 1994). As an example that the reaction energetics is not the only factor controlling the product yield, let us mention the study of the $Ba(^1P_1) + CH_3OH$ reaction carried out by de Pujo *et al.* (1993). Table 3 lists the energetics of the $Ba + CH_3OH$ reaction obtained with the values given in this work for $Ba–OCH_3$.

Examination of this table clearly shows that the chemiluminescent BOH channel is more exothermic than the $BaOCH_3$. However de Pujo *et al.* (1993) reported emission

Table 3. Energetics for the $Ba(^1D_2)+CH_3OH$ reaction (adapted from de Pujo *et al.* (1993)).

Reaction		ΔH(eV)
$Ba(^1P_1)+CH_3OH \rightarrow$	$BaOH(A, ^2\Pi_{1/2})+CH_3$	−1·39
	$BaOH(A, ^2\Pi_{2/3})+CH_3$	−1·31
	$BaOH(B)+CH_3$	−1·18
	$BaOCH_3(A, ^2\Pi_{1/2})+H$	−0·13
	$BaOCH_3(A, ^2\Pi_{2/3})+H$	−0·05
	$BaOCH_3(B)+H$	+0·05

from the $BaOCH_3$ only. In addition, following the insertion mechanism suggested by several authors, one may expect a different steric hindrance for the alkaline earth atom insertion into the O–H or CH_3–O bond, leading to different alkoxide or hydroxide yields, respectively, even for those cases having the same reaction exothermicity. There are indications supporting this argument, as for example the study of the $Ba^*(^1P)+CH_3$–O–CH_3 reaction (de Pujo *et al.* 1993), for which no chemiluminescence was detected, although chemiluminescent reactions are very energetically favourable, as for example the reaction $Ba(6s6p\,^1P_1)+CH_3OCH_3 \rightarrow BaOCH_3(A_{1/2})+CH_3$ for which $\Delta H = -1{\cdot}0$ eV.

The reactivity of $Ca(^1S_0, ^3P_j)$ was also studied with peroxide-type molecules under single-collision conditions (Oberlander *et al.* 1991). Different reaction products were found depending on the electronic state of Ca which is involved. A good example of this different dynamical behaviour is that of the $Ca^*+H_2O_2$ reaction, where $Ca(^3P)$ metastables produce CaOH molecules whereas ground state atoms yield predominantly CaO molecules. The corresponding pathways have been rationalized invoking an insertion mechanism, either on the O–H or on the O–O bond and a time competition between dissociation of the intermediate complex and migration of the H atom. The fact that $Ca(^3P)$ atoms give only CaOH could be attributed to the failure of forming a long-lived complex which would facilitate the H migration required for the CaO formation. Conversely, a direct harpooning mechanism was suggested to take place, so that the fast CaOH formation occurs before the H migration.

5.3. *Electronic excitation: symmetry and stereodynamics effects*

The aim of the experiments described in this section is to use the polarized nature of the laser beam, responsible for electronic excitation, to gain a more detailed insight into the collision dynamics, its anisotropic character in particular. Most experiments involving reactive collisions have been conducted under crossed-beam conditions, by rotating the (linear) polarization direction of the laser beam with respect to the collision axis. The latter is the most natural choice to define a reference axis in the molecular frame. Conversely to the situation described above, no change of energy is involved here. However, inelastic and reactive collisions generally present a complementary and simultaneous aspect, as was shown in the pioneering works of Hertel (Hertel *et al.* 1977, Hertel and Storl 1978) and Zare (Rettner and Zare 1981, 1982) or the $Na+H_2$ and $Ca+HCl$, Cl_2 systems respectively.

Lee and co-workers studied the dynamics of the $Ba(6p\,^1P_1)+Cl_2$ system which yields both $BaCl^+ + Cl^-$ reaction products and $Ba^+ + Cl_2^-$ charge transfer products, the two processes being characterized by their chemiionization emission (Davis *et al.* 1990). It was shown that laser excitation to Ba(6p) enhanced the Ba^+ intensity

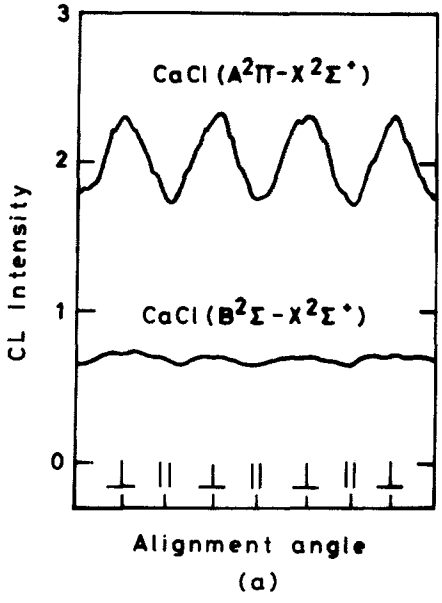

Figure 22. Chemiluminescence emission intensity in the $Ca(^1P_1) + HCl$ reaction as a function of the laser-induced alignment of the p orbital (*a*) $CaCl(A^2\Pi - X^2\Sigma^+)$; (*b*) $CaCl(B^2\Sigma - X^2\Sigma^+)$ (adapted from Rettner and Zare (1982)).

measured in the backward direction of scattering. It was shown that this Ba^+ intensity is maximum when the p-orbital of the barium atom is aligned along the relative velocity vector, as expected from the nature of the electron transfer mechanism.

This result is complementary to those obtained by Zare and co-workers on the $Ca(4p\,^1P_1) + HCl \rightarrow CaCl(A\,^2\Pi, B\,^2\Sigma^+) + H$ reactions, where a weak dependence of the chemiluminescent yield versus alignment of the atomic orbital was observed, for the first time, as is shown in figure 22 (Rettner and Zare 1982). It was found that a parallel alignment of the atom p-orbital along the relative velocity vector enhances the formation of CaCl in the $B\,^2\Sigma^+$ state, whereas a perpendicular one favours formation of the $A\,^2\Pi$ state. This can be understood in the framework of an electron jump model of collision by considering 'outer' and 'inner' harpoonings, the first one, the most efficient, being independent of orbital alignment, whereas the second is not. In this model, the symmetry of the reagent system is conserved, the atom p-orbital transforms into a CaCl molecular orbital and its alignment serves to orientate the reaction products towards the $B\,^2\Sigma^+$ state or towards the $A\,^2\Pi$ one. On the other hand, the $Ca(4p\,^1P_1) + Cl_2$ reaction shows a different behaviour since both $B\,^2\Sigma^+$ and $A\,^2\Pi$ states are favoured by a perpendicular alignment, the Π state in particular. This can be understood from the increased symmetry of the system resulting in an alignment dependence of the outer harpooning, in particular in a C_{2v} geometry of approach. The direct correlation observed between the parallel and perpendicular orbital alignments in the centre-of-mass and the Σ and Π product channels in the laboratory frame, indicates that the behaviour of the system is essentially adiabatic along the reaction path, in agreement with the well-known model of 'orbital following' developed by Hertel (Hertel 1981).

The harpooning model also holds for the $Cs(7p\,^2P) + H_2 \rightarrow CsH + H$ photochemical reaction, for which the ratio of total cross-sections, $\sigma(^2P_{1/2})/\sigma(^2P_{3/2}) \approx 4$, was

measured in a crossed-beam experiment (L'Hermite *et al.* 1991). This 'fine structure effect' could be interpreted and understood in great detail from the calculation of diabatic potential energy surfaces (Gadéa *et al.* 1986) and hemi-quantal dynamics (Gadéa and Durup 1987) in a collinear geometry of approach. Among the $^2\Sigma$ and $^2\Pi$ incoming molecular states, only the former are able to induce the electron jump onto the ionic surface of $^2\Sigma$ symmetry also; at infinite distances between Cs and H_2, the weight of $^2\Sigma$ states is the same for the two channels associated with $Cs(^2P_{1/2})$ and $Cs(^2P_{3/2})$ but, due to dynamical couplings in the entrance valley of the reaction path, the weight of $^2\Sigma$ states at the crossing point between the covalent and the ionic potentials becomes larger for the first channel, giving a higher reaction cross-section to the $Cs(^2P_{1/2})$ level. This result could be confirmed at a more refined level, by considering the hyperfine structure of caesium atoms (Gadéa *et al.* 1988). Here again, the atom reactivity is not totally determined by the potential energy—the lower level of caesium is more reactive than the upper one—but by the symmetry associated with the reagents and products.

5.4. *Van der Waals and cluster reactions*

As is well-known, the physics of supersonic expansions produces very cold molecules which allow for the formation of weakly bound van der Waals molecules (Levy 1980). Early molecular beam studies were limited to gas-phase species where by the use of coexpansion with an inert gas, the amount of cooling could be enhanced, allowing the formation of van de Waals clusters. This technique was used in the early 1970s to study the reactivity of $(CH_3I)_n$ with alkali atoms (González Ureña *et al.* 1974). Partially supersonic expansions could also be obtained with non-volatile materials such as metals, from an effusive metallic beam seeded by a carrier gas (Selby *et al.* 1989). A major advance was implemented by Hertel *et al.* (1977), who produced a supersonic beam of $Na–NH_3$ and $Na–H_2O$ using a 'pick-up' source, where an effusive beam of Na is crossed by a supersonic molecular beam (Schulz *et al.* 1988). Smalley pioneered a method for producing supersonic molecular beams of highly refractory metals such as molybdenum, by the use of a pulsed laser to ablate the material from a solid target in a channel attached to a pulsed high pressure valve (Smalley 1983, Hopkins *et al.* 1983). In the supersonic expansion formed on leaving the channel a variety of metal atoms, van der Waals clusters and molecules can be produced allowing for their study in beam experiments (Hopkins *et al.* 1983, Costes *et al.* 1987, 1988, Jouvet and Soep 1984, Visticot *et al.* 1988, Jouvet *et al.* 1989). Once a well-characterized beam of van der Waals molecules is produced, experiments such as photodepletion (Liu *et al.* 1993), photodissociation and photoionization (Jena *et al.* 1986) can be undertaken, yielding information about the electronic structure of these interesting molecules.

Experiments concerning the reactivity of van der Waals complexes were first carried out by Soep and co-workers (Jouvet and Soep 1984, Jouvet *et al.* 1987, Breckenridge 1989, Soep *et al.* 1991) who studied the dissociation of the complex once excited by a laser pulse, through the action on the LIF spectrum of the product molecule. This approach, which can be viewed as a means to study 'half collisions' of well-defined geometry and symmetry, has been developed for a number of reactive systems including several also studied under crossed-beam conditions. For the reaction of Ca and HCl for example, the Ca–HCl pair is prepared in a supersonic expansion and excited by a laser pulse—at a frequency close to the atomic

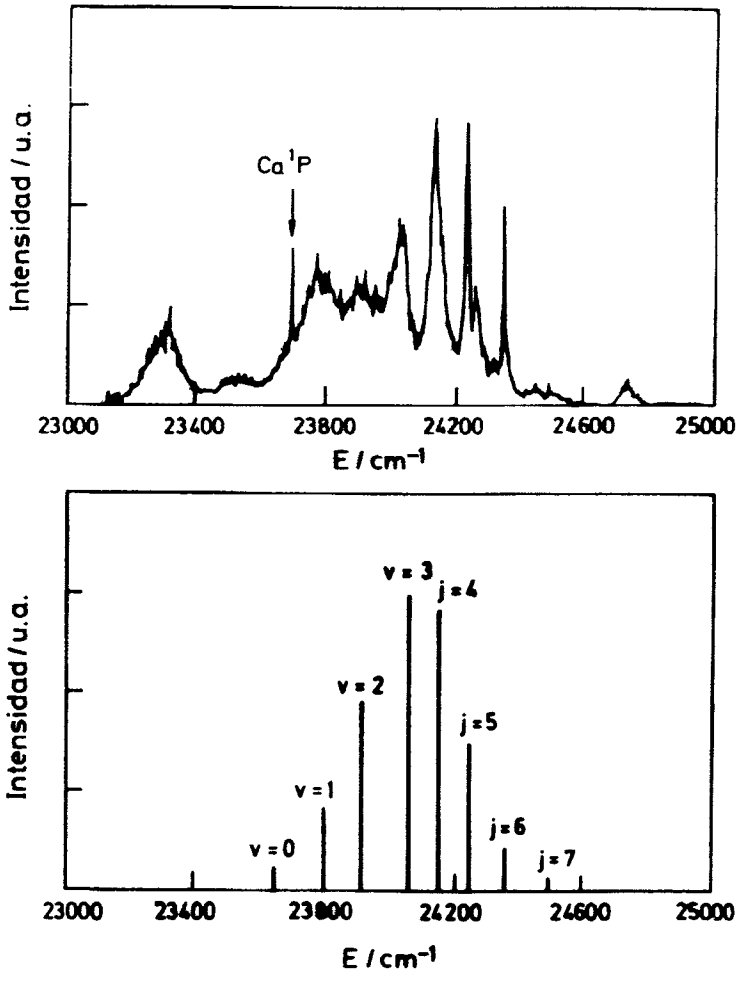

Figure 23. Top: Action spectrum of the chemiluminescent van der Waals Ca...ClH + $h\nu \rightarrow$ CaCl* + H reaction. Bottom: Calculated spectrum using a (hindered rotation) atom–diatom model (adapted from Soep *et al.* (1991)).

resonance—to a repulsive electronic state. The dissociation into CaCl and H products is characterized by tuning the laser frequency and recording the subsequent action spectrum or by use of LIF detection. Figure 23 shows such an action spectrum where the different peaks were assigned and interpreted as local mode excitations, e.g. excitation of perpendicular motions to the reaction coordinate (Soep *et al.* 1991, 1992). Indeed, bending modes or free rotation excitation of van der Waals complexes were assigned and interpreted for the same reactive channel.

On the other hand, the application of ultrafast laser spectroscopy to isolated molecules in pulsed supersonic beam expansions offers the prospect of real-time measurements of the collision complex lifetime. Indeed, this can be accomplished by using the photo-initiated decomposition of van der Waals molecules, as for example IH–CO_2, to monitor the subsequent appearance of OH products according to the successive $H + CO_2 \rightarrow HOCO \rightarrow HO + CO$ reactions (Scherer *et al.* 1987). In these experiments, the lifetime of the HOCO collision complex could be estimated to less

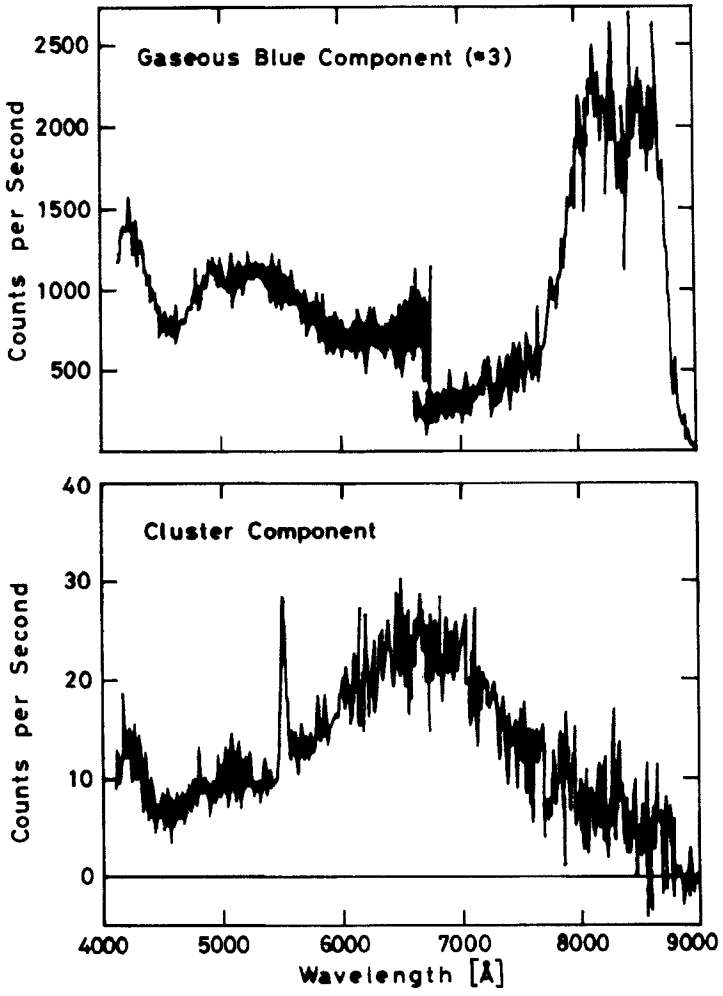

Figure 24. Chemiluminescence spectrum of $Ba+Cl_2$. Top: gas-phase reaction. Bottom: cluster reaction with approximately an average number of 0·25 barium atoms and 1·0 chlorine molecules per cluster. Notice the significant differences between both spectra. See text, adapted from Biquard *et al.* (1995).

than 5 ps, in disagreement with the conclusions obtained by measuring the product angular distribution under crossed-beam conditions. These scattering experiments were conducted at a higher collision energy (about 12 kJ mol^{-1}), providing evidence of a short-lived complex whose lifetime—some 5 ps—is comparable to its rotational period. As has been suggested (Grice 1992), it would be of great interest to determine whether this difference in collision lifetime can be attributed to the increase in collision energy or to the magnitude of the impact parameter, since the reaction in the crossed-beam experiment may arise from much larger impact parameters ($b_{max} \approx 4$ Å) than the photo-initiated van der Waals reaction which arises from a constrained geometry. The high angular momenta of the complex formed in the crossed-beam reaction may also exert a strong influence on its lifetime.

Comparing half-collision reactions in van der Waals complexes with full-collision reactions under crossed-beam conditions and in particular the energy dependence of

the cross-section, is not possible without making important assumptions about the underlying reaction dynamics. One of the main difficulties arises from the different energy resolution of both experiments, another is associated with the impact parameter averaging inherent to crossed-beam experiments which is probably not present in the van der Waals approach. Furthermore, the fundamental question of whether the same region of the potential energy surface is sampled by half-collisions and by full-collisions remains open.

Chemiluminescence produced by the reactive collision of Ba and Cl_2 on an 8000 argon cluster has been recently studied (Biquard *et al.* 1995). In contrast to the gas-phase reaction where it leads to the formation of the radical pair $BaCl^* + Cl$ only, the reaction intermediate $BaCl_2$ was observed as the predominant luminescent channel. Figure 24 shows a comparison between gas (upper graph) and cluster (lower graph) chemiluminescence spectra. Significant differences can be seen in such a comparison. Notice, for example, how the red component of the gas phase has also disappeared in the cluster spectrum. On the other hand, the cluster spectrum shows as dominant feature a continuum which is not present in the gas-phase chemiluminescence. These studies lead to the conclusion that the $BaCl_2^*$ is the only chemiluminescent product. In this view the dominant chemiluminescent reaction $Ba + Cl_2 \rightarrow BaCl_2^*$, closed under gas-phase collision conditions, turns out to be possible because of very efficient trapping of the reaction intermediate by the cluster. As a result, this cluster specificity of trapping, allowing observation of reaction intermediates, opens up new interesting possibilities in the field of reaction dynamics.

6. Concluding remarks

It has been shown how the use of high-resolution optical techniques is greatly improving our knowledge of reaction dynamics, through the full characterization of reaction products and the opening of excited-state reactions, including the study of polarization effects as well as that of van der Waals reactions. For reactive collisions with excited-state atoms, for example, it has been shown that the total energy of the system is not the key parameter but, by contrast, the symmetry of reagents and products appears essential to give account of the dynamics.

Due to the endless development of new tunable laser sources in various optical ranges, there is no doubt that it will be possible to multiply the experimental situations by studying new systems or highly excited ones as a result of various schemes of electronic excitation. In this direction, the study of reactive collisions with Rydberg atoms would provide a new insight into the influence of high angular momenta over elementary chemical processes. Also, the use of circularly-polarized light to study the effect of orbital orientation has not yet been systematized, although promising results were obtained on non-reactive events by Düren (Düren and Hasselbrink 1987) and Leone (1988). Selective electronic excitation could also be achieved for the various isotopes of a given element, as an interesting method of isotopic enrichment using selective chemical reactions (Walther 1976, Zare 1977).

Particularly interesting would be to measure systematically the absolute value of reaction cross-sections in order to compare them with the theoretical estimations provided by quasi-classical or pure quantum calculations. In relation to the analysis of reaction products, it should be mentioned that new interesting possibilities emerge through the use of electronically excited atoms: when looking at the opening of new product channels, one has to consider not only the appearance of electronic manifolds

but also the presence of effects such as spin–orbit interactions, molecular electronic alignment and predissociation processes (Ashfold and Baggott 1987); additional stereodynamics studies associated with pendular states (Loesch and Reincheid 1990, 1991, Friedrich and Herschbach 1991) seem very provising. Related information can be gained from systematic studies of vector correlations through angular momentum conservation in specific systems, i.e. kinematically-constrained reactions (Kin and Herschbach 1987, Zare 1988). Due to the vectorial character of this correlation, new ways of controlling the product spatial distribution would be opened if a diatomic molecule were excited through a parallel transition using a linearly polarized photon; i.e. one can exploit the correlation between $\mathbf{j}'$, $\mathbf{L}'$ and $\mathbf{v}'$ ensuring the $\mathbf{v}'$ vector to appear along the direction of the electric vector associated with the initial laser photon in the laboratory frame.

As mentioned earlier, one can gain insight into the stereodynamics of the bimolecular reactions when laser photodissociation, carried out in a bulb, generates velocity aligned atomic fragments that may subsequently react with target molecules. In fact, photolysis of a molecular precursor in a bulb to produce *hot* atoms has been widely applied to the reaction dynamics field (Flynn and Weston 1986). Recent examples of such applications include the measurement of product rotational alignment, second moments of the differential cross-section, in addition to other state-resolved vector correlation by using the laser-induced fluorescence method (Brouard *et al.* 1993). From the experimental point of view these techniques, based on hot-atom productions in a bulb, have demonstrated the feasibility of measuring product distribution of rotational alignment, second moments of the differential cross-section for state-to-state reactions. Although this novel technique may result in a significant enhancement of signal-to-noise ratios over cross-beam experiments, the results are only applicable for those reactions with favourable mass combination and reaction energetics, as mentioned earlier. In spite of this limitation the technique appears very promising for the measurement of quantum-state specific differential cross-sections which in fact is complementary to information gained from high-resolution crossed-beam scattering.

On the other hand, the advent of ion imaging techniques are of special interest as they can also provide valuable information about quantum-state specific differential cross-sections in a straightforward manner. It should be emphasized that this technique offers several advantages over more traditional methods: (a) by using the resonance-enhanced multiphoton ionization, REMPI technique, a single quantum state of the product can be selected, (b) it shows a high efficiency based on the 4π particle collection that in turn leads to high count rates capable of measuring product angular distribution within a few hours, (c) the technique samples the entire product angular distribution simultaneously. The combination of all these factors may yield the differential cross-section for a single rovibrational quantum state of a molecular product in an elementary reaction.

With regard to the study of chemical reactions in van der Waals molecules and clusters, new studies of chemiluminescent reactions, carried out in clusters, led to the conclusion that very efficient trapping of reaction intermediates can be achieved, and so new possibilities, inaccessible in the gas phase, are opened in the study of reaction dynamics. An interesting method has been developed using the combination of supersonic cooling to produce unreactive van der Waals molecules followed by laser excitation to prepare these excited (reactive) channels. This approach provides not only the clocking for real time experiments in bimolecular (collision complex)

reactions, but also the scenery to study chemical reactions in restricted geometries, e.g. small range of impact parameters. Indeed for those systems having a potential well, the technique is very useful as it provides a way of studying the underlying dynamics of the reactive channels via pump-and-probe action spectra measurements. As an example, let us mention that pumping from the low (non-reactive) potential energy surface to the high (reactive) surface of the van der Waals complex, by scanning a narrow linewidth laser, would allow the study of the collision energy dependence of the induced chemical reaction. Both high spectral and collision energy resolution can be achieved by this attractive method. It should be pointed out that a comparison between the full and half collision methods, although very necessary, still needs to be carried out. The question of whether the van der Waals and crossed-beam reactions really sample the same region of the potential energy surface still remains open.

Finally, two fundamental research fields could find application in applied chemistry. On the one hand, the advent of high intensity, short pulsed tunable lasers could open the way for the 'driving' or 'controlling' of chemical reactions (George 1977, Weiner 1980, Shapiro *et al.* 1988, Brumer and Shapiro 1991). This is the domain of 'laser-assisted collisions' where the laser field is strong enough to interact directly with the collisional complex, in opposition to the situation described above where the laser field prepares the atom, prior to collision. On the other hand, little is known about surface reactions involving electronically excited species (Zhu *et al.* 1991). In this direction, the new field of surface photochemistry could constitute one of the most promising research activities, when solid state physics, laser spectroscopy and gas-phase collision dynamics merge to give the necessary background to understand the underlying elementary chemical processes at surfaces.

Acknowledgments

The authors fully acknowledge the current support of the DGICYT of Spain (grant PB91/357), the French–Spanish cooperation programme (Picasso grant 93071) and the Nato Research Collaborative grant (C.R.G. 950013). AGU especially acknowledges the FBBV Professorship in the Chemistry Department of Cambridge University during which period of time a substantial part of this paper was written. The typing of the manuscript by A. García Sousa is very much appreciated.

References

AKER, P. M., and SLOAN, J. J., 1985, *Time-Resolved Vibrational Spectoscopy*, Springer Proceedings in Physics, edited by A. Laubereau and Stockburger (Berlin: Springer)

ALBERTÍ, M., GIMÉNEZ, X., AGUILAR, A., and GONZÁLEZ UREÑA, A., 1995, *Molec. Phys.*, **5**, 949.

ALTKORN, R., and ZARE, R. N., 1984, *Ann. Rev. phys. Chem.*, **35**, 265.

AOIZ, F. J., HERRERO, V. J., PUENTEDURA, O., and SÁEZ RÁBANOS, V., 1992, *Chem. Phys. Lett.*, **198**, 321.

ARNOLDI, D., and WOLFRUM, J., 1976, *Phys. Chem.*, **80**, 892.

ASHFOLD, M. N. R., and BAGGOTT, J. E., 1987, *Molecular Photodissociation Dynamics* (London: RSC).

AUTROBUS, S., CARD, S. A., HUSAIN, D., LEI, J., CASTANO, F., and SANCHEZ-RAYO, M. N., 1995, *Ber. Bunsenges phys. Chem.*, **99**, 127.

BASTERRECHEA, F., BEITIA, F., CASTAÑO, F., SANCHEZ-RAYO, M. N., SHAUN, C., and HUSAIN, D., 1991, *Phys. Chem.*, **95**, 1615.

BERGMANN, K., 1988, *Atomic and Molecular Beam Methods*, Vol. 1, edited by G. Scoles (Oxford University Press).

BERNSTEIN, R. B., 1982, *Chemical Dynamics via Molecular Beam and Laser Techniques* (Oxford University Press).

BERNSTEIN, R. B., 1984, *Atom-Molecule Collision Theory* (New York: Plenum Press).
BERRY, R. S., RICE, S. A., and ROSS, J., 1980, *Physical Chemistry* (New York: Wiley and Sons).
BILLY, N., GIRARD, B., GOUÉDARD, G., and VIGUÉ, J, 1986, *Recent Advances in Molecular Reaction Dynamics*, edited by R. Vetter and J. Vigué (Paris: Editions du C.N.R.S.).
BILLY, N., GIRARD, B., GOUÉDARD, G., and VIGUÉ, J., 1987, *Molec. Phys.*, **61**, 65.
BILLY, N., GIRARD, B., GOUÉDARD, G., and VIGUÉ, J., 1990, *Laser Chem.*, **10**, 319.
BIQUARD, X., SUBLEMONTIER, O., BERLANDE, J., GAVEAU, M. A., MESTDAGH, J. M., SCHILLING, B., and VISTICOT, J. P., 1995, *J. chem. Phys.*, **92**, 264.
BLAIS, N. C., and TRUBLAR, D. G., 1983, *Chem. Phys. Lett.*, **102**, 120.
BRAS, N., 1990, *Laser Chem.*, **10**, 405.
BRAS, N., JEANNET, J. C., BUTAUX, J., and PERRIN, D., 1991, *J. chem. Phys.*, **95**, 1006.
BRECKENRIDGE, W. J., 1989, *Acts. chem. Res.*, **22**, 21.
BRECKENRIDGE, W. H., and UMEMOTO, H., 1981, *J. chem. Phys.*, **75**, 4153.
BRECKENRIDGE, W. H., and UMEMOTO, H., 1984, *J. chem. Phys.*, **80**, 4168.
BROUARD, M., DUXON, S. P., ENRIQUEZ, P. A., SAYOS, R., and SIMONS, J. P., 1991, *J. phys. Chem.*, **95**, 8169.
BROUARD, M., DUXON, S. P., ENRIQUEZ, P. A., and SIMONS, J. P., 1993, *J. chem. Soc. Faraday Trans.*; 1992, *J. chem. Phys.*, **97**, 7414.
BRUMER, P., and SHAPIRO, M., 1991, *Acts. chem. Res.*, **22**, 407.
CAMPARGUE, R., LEBÉHOT, A., and LEMONNIER, J. C., 1981, *Rarefied Gas Dynamics*, edited by L. Potter (New York: AIAA).
CAMPBELL, M. L., and DAGDIGIAN, P. J., 1986, *J. chem. Phys.*, **85**, 4453.
CHANDLER, D. W., and HOUSTON, P. L., 1987, *J. chem. Phys.*, **87**, 279.
CHILD, M. S., 1974, *Molecular Collision Theory* (New York: Academic Press).
COSTES, M., NAULIN, C., DORTHE, G., and NOUCHI, E. G., 1988, *Selectivity in Chemical Reactions*, edited by J. C. Whitehead (Dordrecht: Kluwer Academic Pulishers).
COSTES, M., NAULIN, C., DORTHE, G., VAUCAMPS, C., and NOUCHI, E. G., 1987, *Faraday Discuss. Chem. Soc.*, **84**, 75.
CRUSE, H. W., DAGDIGIAN, P. J., and ZARE, R. N., 1973, *Faraday Discuss. Chem. Soc.*, **55**, 277.
DAGDIGIAN, P. J., 1978, *Chem. Phys. Lett.*, **55**, 239.
DAGDIGIAN, P. J., and CAMPBELL, M. L., 1987, *Chem. Rev.*, **87**, 1.
DAVIS, H. F., SUITS, A. G., HOU, H., and LEE, Y. T., 1990, *Ber. Bunsenges phys. Chem.*, **94**, 1193.
DEMTRÖDER, W., 1982, *Laser Spectroscopy*, edited by W. Demtröder (Berlin: Springer-Verlag).
DEMTRÖDER, W., 1992, *Atomic and Molecular Beam Methods*, Vol. 2, edited by G. Scoles (Oxford University Press).
DE PUJO, P., SUBLEMONTIER, O., VISTICOT, J-P., BERLANDE, J., CUVELIER, J., ALCARAZ, C., GUSTAVSSON, T., MESTDAGH, J.-M., and MEYNADIER, P., 1993, *J. chem. Phys.*, **99**, 2533.
DE VRIES, M. S., STDANOV, V. I., HANRAHAN, C. P., and MARTIN, R. M., 1983, *J. chem. Phys.*, **78**, 5582.
DIXON, R. N., 1986, *J. chem. Phys.*, **85**, 1866.
DRUET, S. A. J., and TARAN, J. P., 1981, *Prog. quant. Electr.*, **7**, 1.
DÜREN, R., and HASSELBRINK, E., 1987, *J. phys. Chem.*, **91**, 5455.
FARADAY DISCUSSIONS, 1993, *Dynamics at the Gas–Solid Interface*, No. 96.
FARADAY TRANSACTIONS, 1993, Orientation and Polarization Effects in Chemical Reaction Dynamics, *J. Chem. Soc.*, **89**, Nr. 10.
ESTEBAN, M., GARAY, M., GARCIA-TIJERO, J. M., VERDASCO, E., and GONZÁLEZ UREÑA, A., 1994, *Chem. Phys. Lett.*, **230**, 525.
FLUENDY, M. A. D., and LAWLEY, K. P., 1973, *Chemical Application of Molecular Beam Scattering* (London: Chapman and Hall).
FLYNN, G. W., and WESTON, R. E., 1986, *Ann. Rev. phys. Chem.*, **37**, 551.
FREIDRICH, B., and HERSCHBACH, D. R., 1991, *Z. Phys.* D, **18**, 153.
GADÉA, F. X., and DURUP, J., 1987, *Chem. Phys. Lett.*, **138**, 43.
GADÉA, F. X., L'HERMITE, J. M., RAHMAT, G., and VETTER, R., 1988, *Chem. Phys. Lett.*, **151**, 183.
GADÉA, F. X., SPIEGELMANN, F., PÉISSIER, M., and MALRIEU, J. P., 1986, *J. chem. Phys.*, **84**, 4872.
GARAY, M., ESTEBAN, M., VERDASCO, E., and GONZÁLEZ UREÑA, A., 1995, *Chem. Phys.*, **195**, 235.

GAUBATZ, U., RUDECKI, P., BECKER, M., SCHIEMANN, S., KULZ, M., and BERGMANN, K., 1989, *Chem. Phys. Lett.*, **149**, 463.
GEORGE, T. F., 1977, *Theoretical Aspects of Laser Radiation and its Interaction with Atomic and Molecular Systems* (University of Rochester NSF).
GERITY, D. P., and VALENTINI, J. J., 1983, *J. chem. Phys.*, **79**, 5202.
GIRARD, B., 1987, Thèse de Doctorat, Université de Paris (unpublished).
GIRARD, B., BILLY, N., GOUÉDARD, G., and VIGUÉ, J., 1991, *Europhysics Lett.*, **14**, 13; see also the Abstracts of the Seventh European Conference on the Dynamics of Molecular Collisions, Assisi, 1988.
GONZÁLEZ UREÑA, A., 1987, *Adv. chem. Phys.*, **66**, 213.
GONZÁLEZ UREÑA, A., 1991, *Cinética y Dinámica Química Molecular* (Madrid: Eudema).
GONZÁLEZ UREÑA, A., BERNSTEIN, R. B., and PHILLIPS, R. G., 1974. *J. chem. Phys.*, **62**, 1818.
GONZÁLEZ UREÑA, A., and VETTER, R., 1993, *Comments at. mol. Phys.*, **29**, 97.
GONZÁLEZ UREÑA, A., and VETTER, R., 1995, *J. chem. Soc. Faraday Trans.*, **91**, 389.
GREENE, C. H., and ZARE, R. N., 1982, *Ann. Rev. phys. Chem.*, **33**, 119.
GRICE, R., 1992, *Nature*, **359**, 584.
HARTREE, W. S., SIMONS, J. P., and GONZÁLEZ UREÑA, A., 1990, *J. chem. Soc. Faraday Trans.*, **86**, 17.
HEFTER, U., and BERGMANN, K., 1988, *Atomic and Molecular Beam Methods*, Vol. 1, edited by G. Scoles (Oxford University Press).
HENNESSY, H., ONO, Y., and SIMONS, J. P., 1981, *Molec. Phys.*, **43**, 181.
HERING, P., BROOKS, P. R., CURL, R. F., JODSON, R. S., and LOWE, R. S., 1980, *Phys. Rev. Lett.*, **44**, 687.
HERTEL, I. V., 1981, *Adv. chem. Phys.*, **45**, 341.
HERTEL, I. V., HOFMAN, H., and ROST, K. A., 1977, *Phys. Rev. Lett.*, **38**, 343.
HERTEL, I. V., HOFMAN, H. and ROST, K. A., 1979, *J. chem. Phys.*, **71**, 674; see also REILAND, W., TITLES, U., and HERTEL, I. V., 1982, *Phys. Rev. Lett.*, **48**, 1389.
HERTEL, I. V., and REILAND, W., 1981, *J. chem. Phys.*, **74**, 6757.
HERTEL, I. V., and STORL, W., 1978, *Adv. atom. Molec. Phys.*, **13**, 113.
HOPKINS, J. B., LANGRIDGE-SMITH, P. R. R., MORSE, M. D., and SMALLEY, R. E., 1983, *J. Chem. Phys.*, **78**, 1627.
HUSAIN, D., and ROBERTS, G., 1989, *Bimolecular Collisions*, edited by M. N. R. Ashfold and J. E. Baggott (London: RSC)
IRVIN, J. A., and DAGDIGIAN, P. J., 1981, *J. chem. Phys.*, **74**, 6178.
JACOBS, D. C., MADIX, R. J., and ZARE, R. N., 1986, *J. chem. Phys.*, **85**, 5469.
JACOBS, D. C., and ZARE, R. N., 1986, *J. chem. Phys.*, **85**, 5457.
JACQUINOT, P., 1976, *High-Resolution Laser Spectroscopy*, edited by K. Shimoda (Berlin: Springer-Verlag).
JENA, P., RAO, B. K., and KHANNA, S. N., editors, 1986, *The Physics and Chemistry of Small Clusters*, NATO Asi Series (New York: Plenum Publishing Corporation).
JOHNSON, K., KVARAN, A., and SIMONS, J. P., 1983, *Molec. Phys.*, **50**, 981.
JOHNSON, K., PEASE, R., and SIMONS, J. P., 1984, *Molec. Phys.*, **4**, 955.
JONAH, C. D., ZARE, R. N., and OTTINGER, C., 1972, *J. chem. Phys.*, **56**, 263.
JOUVET, C., BOIVINEAU, M., DUVAL, M. C., and SOEP, B., 1987, *J. phys. Chem.*, **91**, 5416.
JOUVET, C., and SOEP, B., 1984, *J. chem. Phys.*, **80**, 2229.
JOUVET, C., SOEP, B., BRECKENRIDGE, W. H., WHITHAM, C., and VISTICOT, J. P., 1989, *J. chem. Soc. Faraday Trans.*, **85**, 113.
KIN, S. K., and HERSCHBACH, D. R., 1987, *Faraday Discuss. Chem. Soc.*, **84**, 159.
KINSEY, J. L., 1977, *J. chem. Phys.*, **66**, 2560.
KITSOPOULOS, T. N., BUNTINE, M. A., BALDWIN, D. P., ZARE, R. N., and CHENDLER, D. W., 1993, *Science*, **260**, 1605.
L'HERMITE, J. M., 1992, *J. chem. Phys.*, **97**, 6215.
L'HERMITE, J. M., RAHMAT, G., and VETTER, R., 1990, *J. chem. Phys.*, **93**, 434.
L'HERMITE, J. M., RAHMAT, G., and VETTER, R., 1991, *J. chem. Phys.*, **95**, 3347.
LEE, Y. T., 1988, *Atomic and Molecular Beam Methods*, Vol. 1, edited by G. Scoles (Oxford University Press), pp. 553–569.
LEONE, S. R., 1988, *Selectivity in Chemical Reactions*, edited by J. C. Whitehead (Dordrecht: Kluwer Academic Publishers).

LEVINE, R. D., and BERNSTEIN, R. B., 1987, *Molecular Reaction Dynamics and Chemical Reactivity* (Oxford University Press).
LEVY, D. H., 1980, *Quantum Dynamics of Molecules*, edited by R. G. Woolley (New York: Plenum).
LI, RUN-JUN., HAN, KE-LI., LI, FU-E., LU, RI-CHANG., HE, GUO-ZHONG., LOU, NAN-QUAN., 1994, *Chem. Phys. Lett.*, **220**, 281.
LIN, K. C., and CHANG, H. C., 1989, *J. chem. Phys.*, **90**, 6151.
LIU, K., POLANYI, J. C., and YANG, S., 1993, *J. chem. Phys.*, **98**, 5431.
LOESCH, H. J., 1986, *Chem. Phys.*, **104**, 213.
LOESCH, H. J., and REINCHEID, A., 1990, *J. chem. Phys.*, **94**, 4779.
LOESCH, H. J., and REINCHEID, A., 1991, *J. phys. Chem.*, **95**, 8194.
MARINERO, E. E., RETTNER, C. T., and ZARE, R. N., 1984, *J. chem. Phys.*, **80**, 4142.
MCCLELLAND, M., and HERSCHBACH, D. R., 1978, *Molec. Phys*, **35**, 541.
MEIER, W., ROTTKE, H., ZACHARIAS, H., and WELGE, K. H., 1985, *J. chem. Phys.*, **83**, 4360.
MENÉNDEZ, M., GARAY, M., VERDASCO, E., and GONZÁLEZ UREÑA, A., 1993, *J. chem. Soc. Faraday Trans.*, **89**, 1493.
MENZINGER, M., 1988, *Selectivity in Chemical Reactions*, edited by J. C. Whitehead (Dordrecht: Kluwer Academic Publishers).
MESTDAGH, J. M., ALCARAZ, C., BERLANDE, J., CUVELLIER, J., GUSTAVSSON, T., MEYNADIER, P, DE PUJO, P., SUBLEMENTIER, O., and VISTICOT, J. P., 1990, *Laser Chem.*, **10**, 389.
MESTDAGH, J. M., BALKO, B. A., COVINSKY, M. H., WEISS, P. S., VERNON, M. F., SCHMID, H., and LEE, Y. T., 1987, *Faraday Discuss. Chem. Soc.*, **84**, 145.
MESTDAGH, J. M., VISTICOT, J. P., and SUITS, A. G., 1994, *The Chemical Dynamics and Kinetics of Small Radicals*, edited by K. Liu and A. Wagner (Singapore: World Scientific Publishing).
MILLER, D. R., 1988, *Atomic and Molecular Beam Methods*, Vol. 1, edited by G. Scoles (Oxford University Press).
MIMS, C. A., and BROPHY, J. A., 1977, *J. chem. Phys.*, **66**, 1378.
MOSKOWITZ, W. P., STEWART, B., BILOTTA, R. M., KINSEY, J. L., and PRITCHARD, D. E., 1984, *J. chem. Phys.*, **80**, 5496.
MOTZKUS, M., PILCHLER, G., CORREIA, R. R. B., CUNHA, S. L., KOMPA, K. L., and HERRING, P., 1992, *Coherent Raman Spectroscopy: applications and developments* (Singapore: World Scientific Publishing).
MURPHY, E. J., BROPHY, J. H., ARNOLD, G. S., DIMPFL, W. L., and KINSEY, J. L., 1979, *J. chem. Phys.*, **70**, 5910.
NAULIN, CH., COSTES, M., MOUDDEN, Z., GHANEM, N., and DORTHE, G., 1993, *Chem. Phys. Lett.*, **202**, 452.
NIEH, J. C., and VALENTINI, J. J., 1988, *Phys. Rev. Lett.*, **60**, 519.
NIEH, J. C., and VALENTINI, J. J., 1990, *J. chem. Phys.*, **92**, 1083.
NODA, C., MCKILOP, J. S., JOHNSON, M. A., WALDECK, J. R., and ZARE, R. N., 1986, *J. chem. Phys.*, **85**, 856.
OBERLANDER, M. D., KAMPF, R. P., and PARSON, J. M., 1991, *Chem. Phys. Lett.*, **176**, 385.
ODIORNE, T. J., BROOKS, P. R., and KASPER, J. V., 1971, *J. chem. Phys.*, **55**, 1980.
OHOYAMA, H., IGURO, T., KASAI, T., and KUWAKA, K., 1993, *Chem. Phys. Lett.*, **209**, 361.
PARSON, J. M., and FANG, C. C., 1990, *J. chem. Phys.*, **92**, 4823.
PAULY, H., 1988, *Atomic and Molecular Beam Methods*, Vol. 1, edited by J. Scoles (Oxford University Press).
PHILLIPS, W. D., SERRI, J. A., ELY, D. J., PRITCHARD, D. E., WAY, K. R., and KINSEY, J. L., 1978, *Phys. Rev. Lett.*, **41**, 937.
PICHLER, G., MOTZKUS, M., CUNHA, S. L., CORREIA, R. R. B., KOMPA, K. L., and HERRING, P., 1992, *Il Nuovo Cimento*, **14**, 1065.
POLANYI, M., 1932, *Atomic Reactions* (London: Williams and Morgete).
POLANYI, J. C., and SCHREIBER, J. L., 1974, *Physical Chemistry, An Advanced Treatise*, vol. VI A, edited by W. Jost (New York: Academic Press).
PRISANT, M. G., RETNER, C. T., and ZARE, R. N., 1981, *J. chem. Phys.*, **75**, 2222.
PRISANT, M. G., and ZARE, R. N., 1985, *J. chem. Phys.*, **83**, 5458.
RAHMAT, G., VERGÈS, J., VETTER, R., GADÉA, F. X., PÉLISSIER, M., and SPIEGELMANN, F., 1986, *Recent Advances in Molecular Reaction Dynamics*, edited by R. Vetter and J. Vigué (Paris: Editions du CNRS).

RETTNER, C. T., and ZARE, R. N., 1981, *J. chem. Phys.*, **74**, 3630.
RETTNER, C. T., and ZARE, R. N., 1982, *J. chem. Phys.*, **77**, 2416.
SCHERER, N. F., KHUNDKAR, L. R., BERNSTEIN, R. B., and ZEWAIL, A. H., 1987, *J. chem. Phys.*, **87**, 145.
SCHIEMANN, S., KAHM, S., STEUERWALD, S., and BERGMANN, K., 1993, *Phys. Rev. Lett.*, **71**, 3637.
SCHINKE, R., 1993, *Photodissociation Dynamics* (Cambridge University Press).
SCHULZ, C. P., HAUGSTÖTTER, R., TITTES, H. U., and HERTEL, I. V., 1988, *Z. Phys.* D., **10**, 279.
SCOLES, G., editor, 1988, *Atomic and Molecular Beam Methods*, Vol. 1 (Oxford University Press).
SELBY, K., VOLLMER, M., MASUI, J., HEER, W. A., and KNIGHT, W. D., 1989, *Phys. Rev.* B **40**, 5417.
SERRI, J. A., BECKER, C. H., ELBEL, M. B., KINSEY, J. L., MOSKOWITZ, W. P., and PRITCHARD, D. E. P., 1981a, *J. chem. Phys.*, **74**, 5116.
SERRI, J. A., KINSEY, J. L., and PRITCHARD, D. E., 1981b, *J. chem. Phys.*, **75**, 663.
SHAPIRO, M., HEPBURN, J. W., and BRUMER, P., 1988, *Chem. Phys. Lett.*, **149**, 451.
SHATTER, N. E., and BERSHOM, R., 1991, *J. chem. Phys.*, **94**, 4817.
SHATTER, N. E., ORT-EWING, A. J., SIMPSON, W. R., XU, R., and ZARE, R. N., 1993, *Chem. Phys. Lett.*, **212**, 155.
SHIMODA, K., 1976, *High-Resolution Laser Spectroscopy* (Berlin: Springer-Verlag).
SIEGEL, A., and SCHULTZ, A., 1978, *Chem. Phys.*, **28**, 265.
SIMPSON, W. R., ORT-EWING, A J., and ZARE, R. N., 1993, *Chem. Phys. Lett.*, **212**, 163.
SMALLEY, R. E., 1983, *Laser Chem.*, **2**, 167.
SMITH, I. W. M., 1980, *Kinetics and Dynamics of Elementary Gas Reactions* (London: Butterworths).
SMITH, N., SCOTT, T. P., and PRITCHARD, D. E., 1984, *J. chem. Phys.*, **81**, 1229.
SOEP, B., ABBES, S., KELLER, A., and VISTICOT, J. P., 1992, *J. Chem. Phys.*, **96**, 440.
SOEP, B., WHITHAM, C. J., KELLER, A., and VISTICOT, J. P., 1991, *Faraday Discuss. Chem. Soc.*, **91**, 191.
STOLTE, S., 1988, *Atomic and Molecular Beam Methods*, Vol. 1, edited by G. Scoles (Oxford University Press), pp. 631–652.
STOLTE, S., PROCTOR, A. E., POPE, W. M., and BERNSTEIN, R. B., 1977, *J. chem. Phys.*, **66**, 3468.
SUITS, A. G., BONTUYAN, L. S., HOUSTON, P. L., and WHITAKER, B. J., 1992, *J. chem. Phys.*, **96**, 8618.
TAN, A., MOE, G., and HAPPER, W., 1975, *Phys. Rev. Lett.*, **35**, 1630.
TOENNIES, J. P., 1974, *Physical Chemistry, An Advanced Treatise*, VI A, edited by W. Jost (New York: Academic Press).
TSUKIYAMA, K., KATA, M. B., and BERSHOHM, R., 1980, *J. chem. Phys.*, **84**, 1934.
VAN DER ZANDE, W. J., ZHANG, R., ZARE, R. N., MCKENDRICK, K. G., and VALENTINI, J. J., 1991, *J. phys. Chem.*, **95**, 8205.
VERDASCO, E., and GONZÁLEZ UREÑA, A., 1990, *Chem. Phys. Lett.*, **169**, 437.
VERDASCO, E., and GONZÁLEZ UREÑA, A., 1991, *J. chem. Phys.*, **93**, 426.
VERDASCO, E., MENÉNDEZ, M., GARAY, M., GONZÁLEZ UREÑA, A., BENOIST D'AZY, O., POBLETE, F. J., and TAIEB, G., 1992, *Laser Chem.*, **12**, 123.
VERDASCO, E., SÁENZ RÁBANOS, V., AOIZ, F. J., and GONZÁLEZ UREÑA, A., 1987, *J. phys. Chem.*, **91**, 2073.
VERDASCO, E., SÁEZ RÁBANOS, V., and GONZÁLEZ UREÑA, A., 1989, *Laser Chem.*, **10**, 51.
VERNON, M. F., SCHMIDT, H., WEISS, P. S., COVINSKY, M. H., and LEE, Y. T., 1986, *J. Chem. Phys.*, **84**, 5580.
VISTICOT, J. P., SOEP, B., and WHITHAM, C. J., 1988, *J. phys. Chem.*, **92**, 4574.
WALTHER, H., 1976, *Laser Spectroscopy of Atoms and Molecules*, edited by H. Walther (Berlin: Springer-Verlag).
WEINER, J., 1980, *J. chem. Phys.*, **72**, 2856.
WEISS, P. S., MESTGAGH, J. M., SCHMIDT, H., VERNON, M. F., COVINSKY, M. H., BALKO, B. A., and LEE, Y. T., 1986, *Recent Advances in Molecular Reaction Dynamics*, edited by R. Vetter and J. Vigué (Paris: Editions du CNRS).
WHITEHEAD, J. C., 1988 *Selectivity in Chemical Reactions* (Dordrecht: Kluwer Academic Publishers).
WICKE, B. G., 1983, *J. chem. Phys.*, **78**, 6036.

YUH, H. J., and DAGDIGIAN, P. J., 1983, *J. chem. Phys.*, **79**, 2086.
ZANDEE, L., and BERNSTEIN, R. B., 1978, *J. chem. Phys.*, **68**, 3760.
ZARE, R. N., 1972, *Molec. Photochem.*, **4**, 1.
ZARE, R. N., 1977, *Scient. Amer.*, **236** (2), 86.
ZARE, R. N., 1979, *Faraday Discuss. Chem. Soc.*, **67**, 7.
ZARE, R. N., 1988, *Angular Momenta* (New York: Wiley and Sons).
ZEWAIL, A. H., 1988, *Science*, **2423**, 1645.
ZEWAIL, A. H., 1989, *J. chem. Soc. Faraday Trans.*, **85**, 1221.
ZHU, X. Y., WHITE, J. M., WOLF, M., HASSELBRINK, E., and ERTL, G., 1991, *J. phys. Chem.*, **95**, 8393.